Semi-Annual Progress Report

NASA Grant NGR 14-005-200

"Studies of Discharge Mechanisms in High Pressure Gases-Applications to High Efficiency High Power Lasers"

Prepared for
National Aeronautics and Space Administration
NASA - Lewis Research Center

1 November 1975

B. F. Cherrington
J. T. Verdeyen
J. G. Eden
S. Leslie

Gaseous Electronics Laboratory
Department of Electrical Engineering
University of Illinois at Urbana-Champaign
Urbana, Illinois 61801

Semi-Annual Progress Report

NASA Grant NGR 14-005-200

"Studies of Discharge Mechanisms in High Pressure Gases-Applications to High Efficiency High Power Lasers"

Prepared for
National Aeronautics and Space Administration
NASA - Lewis Research Center

1 November 1975

B. F. Cherrington
J. T. Verdeyen
J. G. Eden
S. Leslie

Gaseous Electronics Laboratory
Department of Electrical Engineering
University of Illinois at Urbana-Champaign
Urbana, Illinois 61801

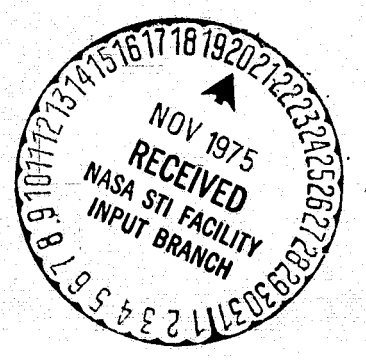

This report consists of the Ph.D. thesis of James Gary Eden and represents the considerable work we have done on optical absorption and flashlamp pumped fluorescence studies in high pressure Cesium-Xenon mixtures. A thorough analysis is made of the excimer systems formed by the combination of excited Cs(7^2S,5^2D) and Xe and their potential application to CsXe laser systems. The modeling of such laser systems forms the basis of our continuing research in order to obtain an optically pumped rare gas-alkali vapor excimer laser.

The appendix referred to in the report has already been reported to NASA in the Semi-Annual Progress Report dated 1 November 1974 and so is not repeated here.

I. INTRODUCTION

Currently, there is considerable interest in developing high efficiency, energetic lasers for such diverse applications as laser induced thermonuclear fusion, isotope separation and optical power transmission. In particular, due to the continuing need for a plentiful, inexpensive energy source, thermonuclear fusion constitutes perhaps the most attractive application for such lasers. However, the criteria demanded of these lasers are stringent: 1) output powers of $\sim 10^{13} - 10^{15}$ watts on nanosecond time scales, 2) efficiencies $\gtrsim$ 30% and 3) operating frequencies in the visible portion of the spectrum. Unfortunately, lasers supplying these qualifications do not presently exist. For instance, both the CO_2 and CO lasers, while exhibiting excellent efficiencies, operate at infrared wavelengths ($\sim$ 5 - 10μ) and do not presently produce sufficient energies to efficiently initiate the thermonuclear reaction.

For several years, a new class of diatomic molecules that promises to yield lasers with the desired properties has been under extensive investigation. These molecules are characterized by a repulsive ground state and at least one bound excited energy level (cf. Fig. 1). Transitions in such weakly bound molecules are possible from this bound state to ground where subsequent dissociation of the molecule occurs in $\sim 10^{-13}$ sec (1 vibrational period). Clearly, then, the repulsive ground state facilitates obtaining stimulated

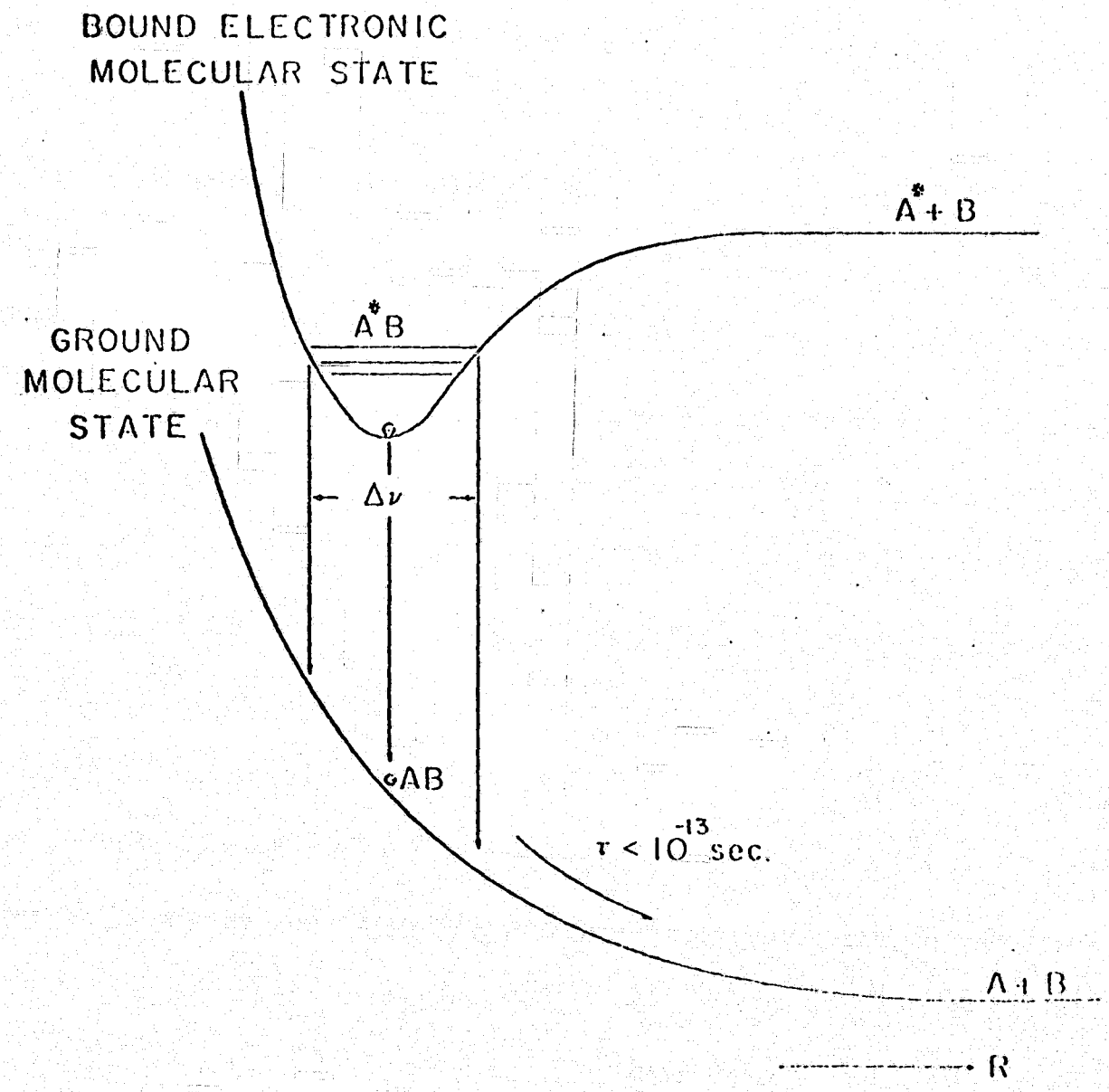

Fig. 1. Potential energy level diagram of the bound excited and repulsive ground states for the molecule AB.

emission from these molecules since only small excited molecular state densities are necessary to obtain a population inversion. The magnitude of the threshold excimer density is, however, strongly dependent on the contour of the ground state potential.

Therefore, it is conceivable that large laser energy output at high quantum efficiency ($\frac{\lambda_{ATOMIC}}{\lambda_{MOLECULAR}}$) is attainable in these molecular systems if the necessary population inversion can be realized. Also, as may be seen in Fig. 1, population inversion between the molecular excited and ground states is possible for various interatomic radii which implies the possibility of obtaining laser output that is tunable in wavelength. Molecules, such as those described above, in which stimulated emission has been obtained, are known as excimer or dissociation lasers.

Dissociative lasing was first suggested by Houtermans[1] in 1960 and was originally observed in Xe_2 (see refs. 2-4). Subsequently, stimulated emission has been demonstrated for several other rare-gas homonuclear molecules,[5] the Xe O and Kr O systems[6] and for the rare gas - monohalide molecules (such as Kr F).[7-9] Unfortunately, the majority of these molecules lase in the vacuum ultraviolet (VUV) portion of the spectrum which is undesirable for most interesting applications requiring high energy lasers.

A family of molecules having: 1) the electronic energy level configuration necessary for dissociative lasing and 2) energy level separations in the visible regime are the alkali-rare gas

molecular systems. Phelps[10] has calculated the stimulated emission cross sections for the $A^2\,\Pi \rightarrow X^2\,\Sigma$ transitions for several of these molecules; also, by performing low level excimer fluorescence measurements, Hedges and co-workers[11] have determined the potential energy level diagrams for the Cesium and Rubidium - rare gas molecules. However, presently little is known of: 1) the collisional rates responsible for the formation and destruction of the excited alkali-rare gas molecules or 2) which excimer states might prove to be the most attractive candidates for lasing. It has, therefore, been the purpose of this work to investigate which excimer states are most promising and those physical mechanisms which are crucial to obtaining population inversions in the alkali-rare gas molecules.

The important rate processes are shown in Fig. 2. The atomic state A^* is pumped (optically or through electronic collisions) directly or indirectly through cascade from higher - lying energy levels. Formation of the $(AB)^*$ excimer then proceeds by way of three-body collisions. That is:

$$A^* + 2B \xrightarrow{k_f} (AB)^* + B + KE$$

where the third body is necessary to stabilize the excimer in a bound vibrational state. Knowledge of the magnitude of the rate k_f is important since the three body collision process limits the number of excimers formed per second. Thus, this rate is crucial in

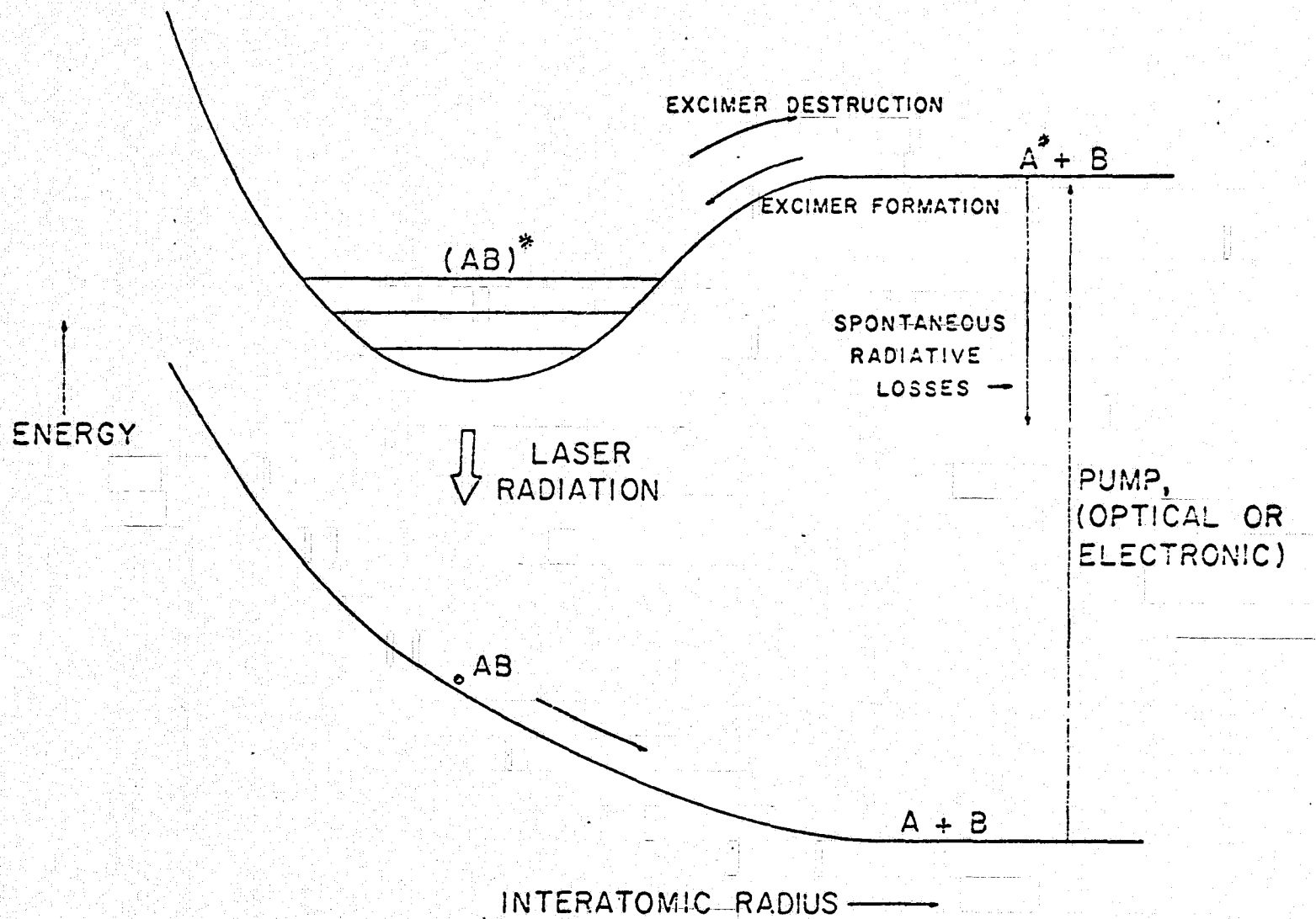

Fig. 2. Energy level diagram for the molecule AB showing the processes important in creating a prospective dissociation laser.

assessing the viability of obtaining stimulated emission from the alkali-rare gas molecule of interest. (Experiments that have been performed to determine the formation rate of the Na Ar excimer are described in the Appendix). Another excited atomic specie decay process which seriously limits the maximum attainable excimer population is atomic spontaneous radiative decay. It is surprising, then, that the majority of present investigations of the optical properties of the alkali-rare gas molecules have concentrated on utilizing low-lying alkali P states to form the alkali-rare gas excimer. Such states may be undesirable due to their short radiative lifetimes ($\sim$ nsec). However, this work summarizes the optical properties of excited states in Cesium-Xenon mixtures that are characterized by relatively long radiative lifetimes and, therefore, may be much more promising as potential laser upper levels. Figure 3 shows a partial energy diagram of Cesium. (Cesium was chosen primarily due to its large vapor pressures at moderate temperatures). In the past, investigators have looked almost exclusively at the Cs-rare gas excimers formed by perturbing the Cs^* ($6^2P_{1/2,3/2}$) states with a ground state rare gas atom. These atomic states are connected to ground by fast radiative transitions at 8521 and 8944 Å which limit the maximum excimer density attainable due to depletion of the excited alkali atomic species. However, note that the Cs^* (7^2S and 5^2D) $\rightarrow$ ground atomic transitions (shown by dashed lines) are normally forbidden due to violation of quantum-mechanical

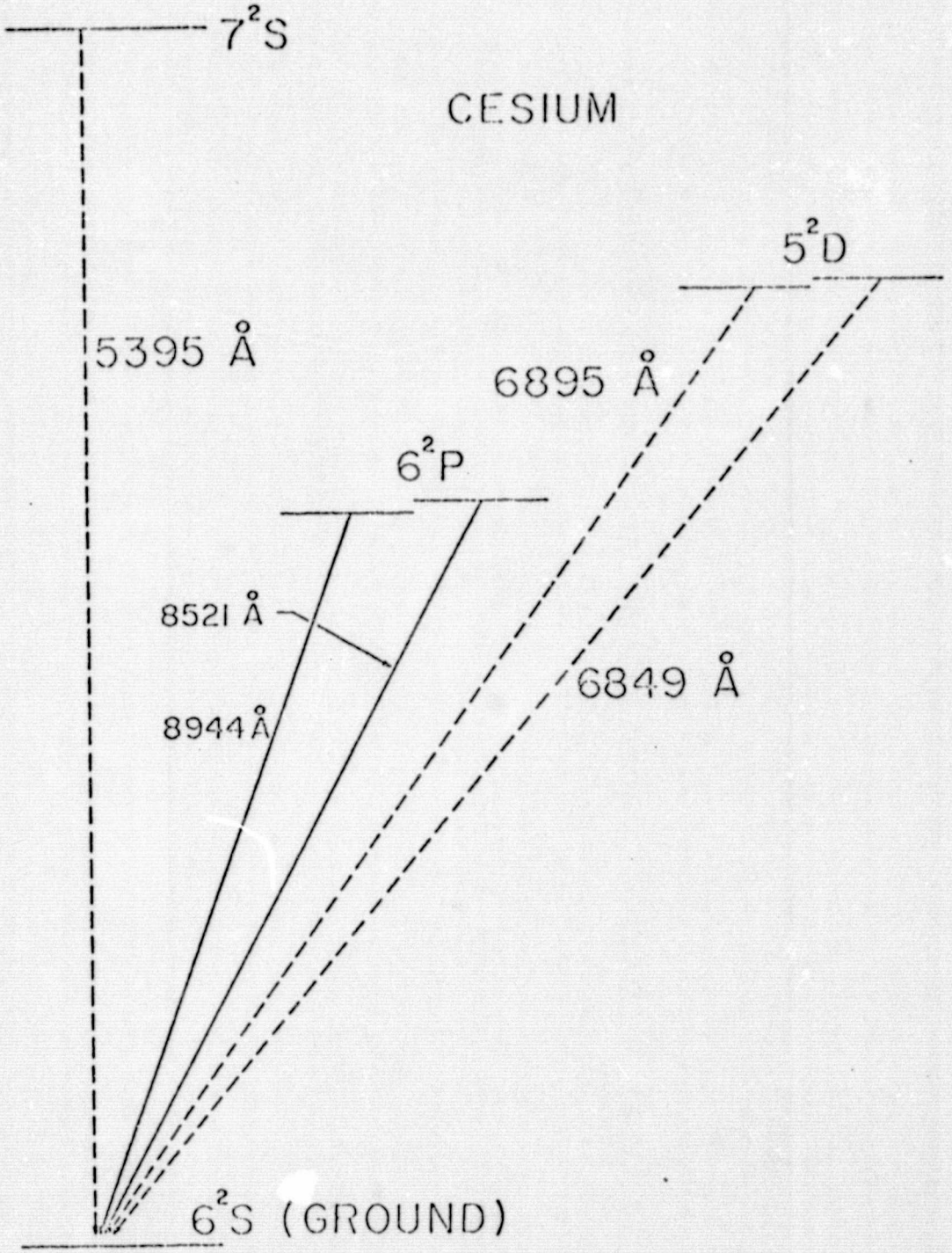

Fig. 3. Partial energy level diagram for atomic Cesium. The forbidden Cs(7^2S, $5^2D \rightarrow 6^2S$) lines at 5395, 6849 and 6895 Å are denoted by dashed lines.

selection rules. Observations to be described later demonstrate that the addition of high pressure Xenon to the Cesium permits these transitions to occur. The lifetimes of these "quasi-forbidden" transitions are considerably longer than for the normal P-S transitions and so better energy storage and population inversion conditions may well be possible in such systems.

Although several observations of absorption and emission on "forbidden" rare gas - perturbed alkali transitions have been reported,[12-15] only recently have alkali S → S transitions been seen in fluorescence. Upon exciting the Cs^* (7^2P) level with an argon-ion laser, Tam et al[16] observed intense $[Cs(7^2S)Xe]^*$ molecular emission.

In this paper, extensive measurements of the $(Cs[7^2S]Xe)^*$ and $(Cs[5^2D]Xe)^*$ molecular absorption spectra in high pressure Cesium-Xenon mixtures are reported for the first time. In addition, flashlamp-pumped fluorescence profiles for these long lived ($\tau > 1$ μsec) molecular states are presented. In particular, the $(Cs[7^2S]Xe)^*$ molecule is found to be attractive as a potential dissociation laser due to its large dissociation energy and stimulated emission cross-section, ($\sigma \sim 10^{-17}$ cm^2). As a result, low threshold population densities have been calculated for this system. Section III discusses the experimental apparatus utilized to measure the Cs-Xe absorption and emission spectra. Typical data runs and their interpretation in terms of a possible CsXe excimer laser are presented in Section IV. Finally, Section V summarizes the results and suggests possible areas for further work.

II. EXPERIMENTAL APPARATUS AND TYPICAL DATA

The experimental apparatus used to obtain the CsXe absorption and fluorescence data is shown schematically in Fig. 4. The pyrex absorption tubes were nominally 15.7 cm long and 2.5 cm o.d. and incorporated fused windows situated normal to the tube's axis. These tubes were chemically cleaned, evacuated to $\sim 5 \cdot 10^{-6}$ Torr and heated under vacuum to insure that the walls were adequately outgassed. Subsequently, they were filled with doubly distilled Cesium and research grade Xenon (99.995% purity) and then sealed off. High Xenon pressures in the absorption vessels were attained by filling the vacuum system manifold with Xenon and immediately condensing the gas into the tube using liquid nitrogen. The tube fill pressure could then be computed using the ideal gas law, knowing the ratio of the manifold to absorption tube volume. Uncertainty in this ratio is responsible for an estimated 20% error in pressure determination.

The Cs-Xe filled vessels were then placed at the center of a highly polished double elliptical cavity. This cavity was constructed so that the center of the cavity coincided with one of the focii of each of the two ellipses. At the other focus of each ellipse was mounted a high intensity ($\sim$ 1.5 MW output/lamp) water-cooled linear Xenon flashtube.

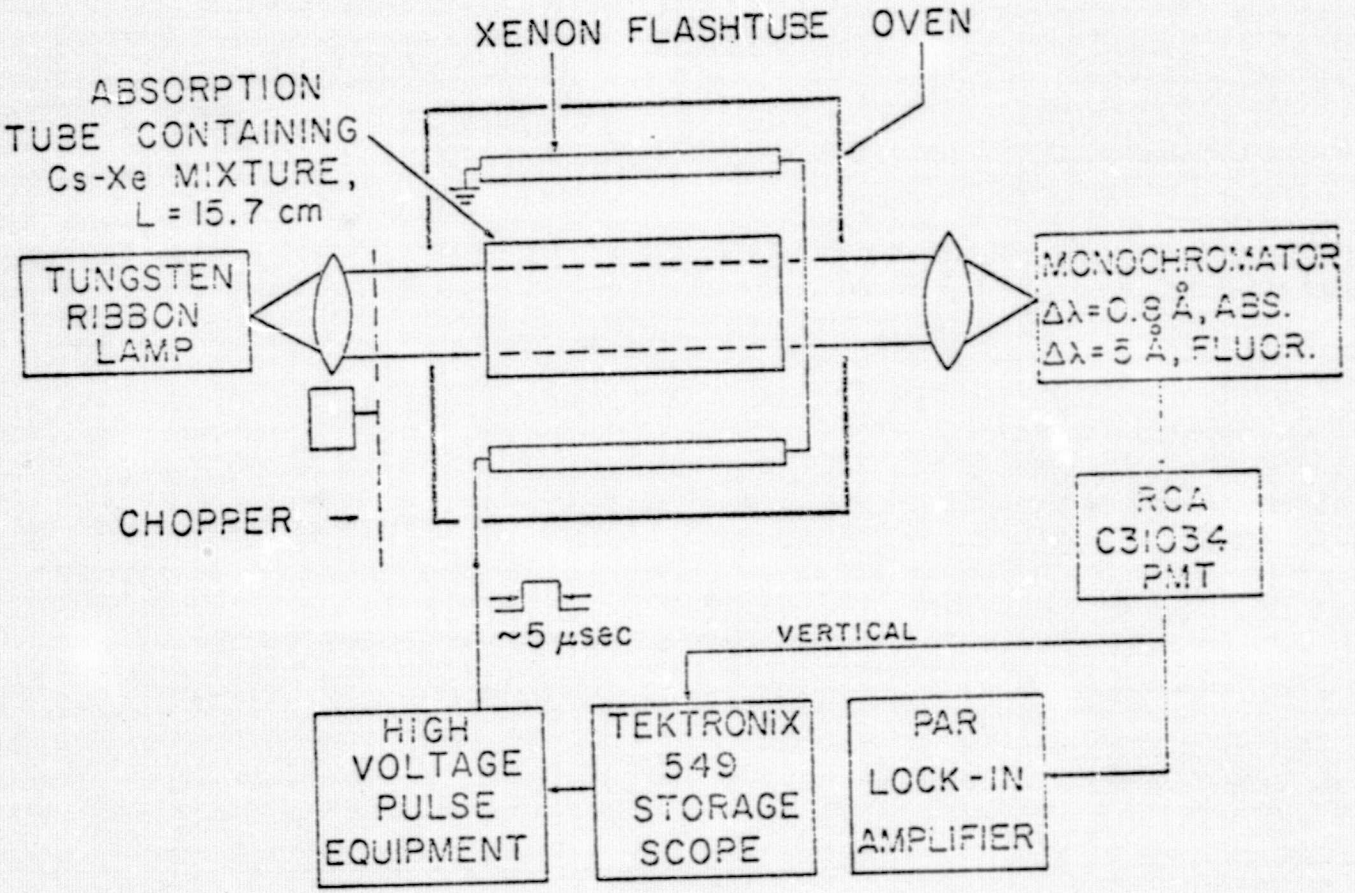

Fig. 4. Schematic diagram of the experimental apparatus used to measure the absorption and fluorescence spectra of Cs-Xe mixtures.

The electrical circuitry responsible for delivering a fast risetime, high voltage pulse to the flashtubes is shown in Fig. 5. This system was comprised of two separate components: 1) the high voltage pulse and 2) simmer circuit. The simmer circuit's sole function was to maintain a low-level (∿ 25 ma) DC arc in the flashtubes. Such an arc reduces the voltage necessary to fire the lamps and enhances flashlamp radiative output repeatability.[17] An 800 nsec rise time, 5 μsec FWHM, 15 kV, ∿ 600 amp electrical pulse was generated in the pulse circuitry by discharging a .1 μf capacitor through an EG&G sparkgap. The triggered output of an EG&G TM-11A pulse unit was employed to activate the sparkgap. Finally, the 8020 vacuum diode prevented the 600 Amp pulse from entering the simmer circuitry.

The Tektronix 514 storage oscilloscope (operated in the single sweep mode) served the dual purpose of triggering the EG&G TM-11A unit and of observing the CsXe fluorescence waveform. The use of the storage capabilities of the scope to display these waveforms made it possible to record the fluorescence peak amplitude (arbitrary units) as a function of wavelength.

For absorption measurements, a standard tungsten ribbon lamp was used as the broad band source. After collimation, the lamp radiation was mechanically chopped before entering the absorption tube. The resulting CsXe absorption spectrum was dispersed by a Heath EU-700 monochromator and detected by an RCA C31034 photo-

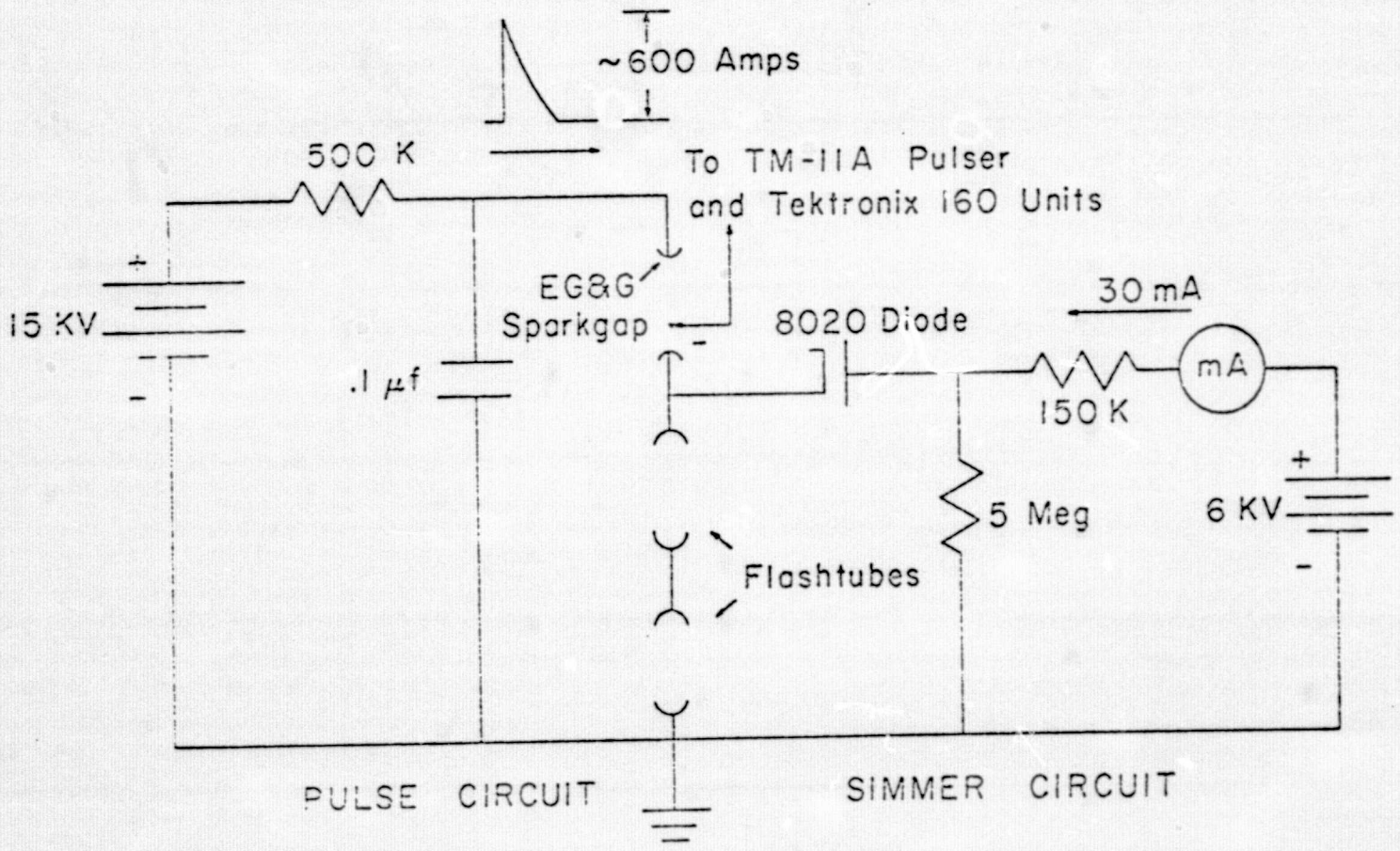

Fig. 5. Schematic diagram of the pulse and simmer circuits for the Xenon flashtubes.

multiplier. Actual data was obtained by scanning the monochromator and recording the synchronous output of a PAR HR-8 lock - in amplifier utilizing a strip-chart recorder. (The wavelength resolution of the detection system, including the effect of the electronics, is shown in Fig. 4). In this way, spectrally resolved absorption and fluorescence profiles were generated for the CsXe energy levels of interest. A typical set of absorption data for the $6^2S \rightarrow 5^2D$ transitions in Cs-Xe mixtures is shown in Fig. 6. Data sets similar to this for various Xenon and Cesium densities* were converted to absorption coefficients using the equation:

$$\alpha(\lambda) = \frac{1}{L} \ln\left[\frac{I_{out}(\lambda)}{I_{in}(\lambda)}\right] \quad , \ cm^{-1}, \qquad (1)$$

where L is the absorption tube length (15.7 cm). The repeatability of this absorption data is displayed in Fig. 7. The absorption coefficient, for fixed Xenon and Cesium densities, is plotted versus wavelength for three superimposed data runs. Fluctuations in the data are < 25% for all wavelengths. Also, due to careful calibration of the monochromator against known atomic transitions in the spectral regions of interest, uncertainty in the detection wavelength is $\pm$ 1 Å.

*Knowing the absorption tube temperature (measured using chromel-alumel thermocouples), the Cesium density was inferred from the vapor pressure curves.

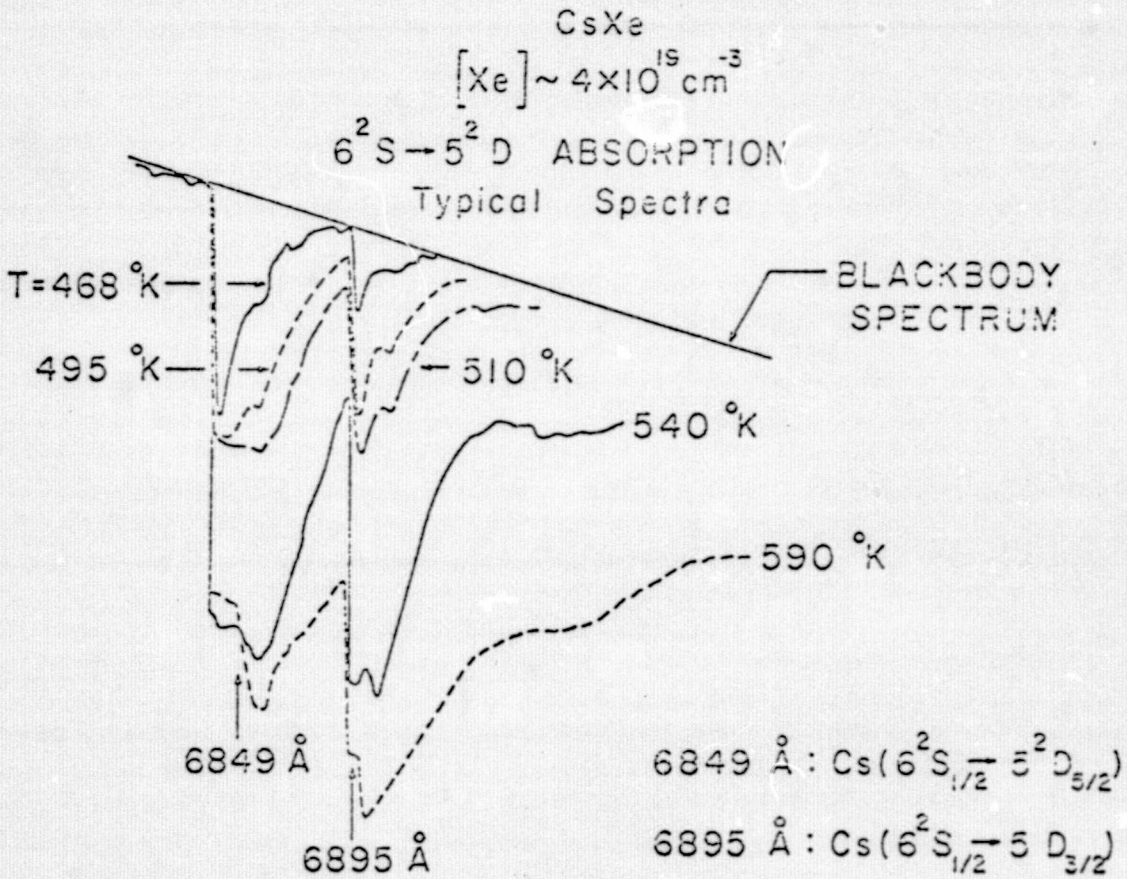

Fig. 6. Typical $6^2S \rightarrow 5^2D$ absorption data shown for various gas temperatures (e.g., Cesium densities) for [Xe] ~ $4 \cdot 10^{19}$ cm^{-3}.

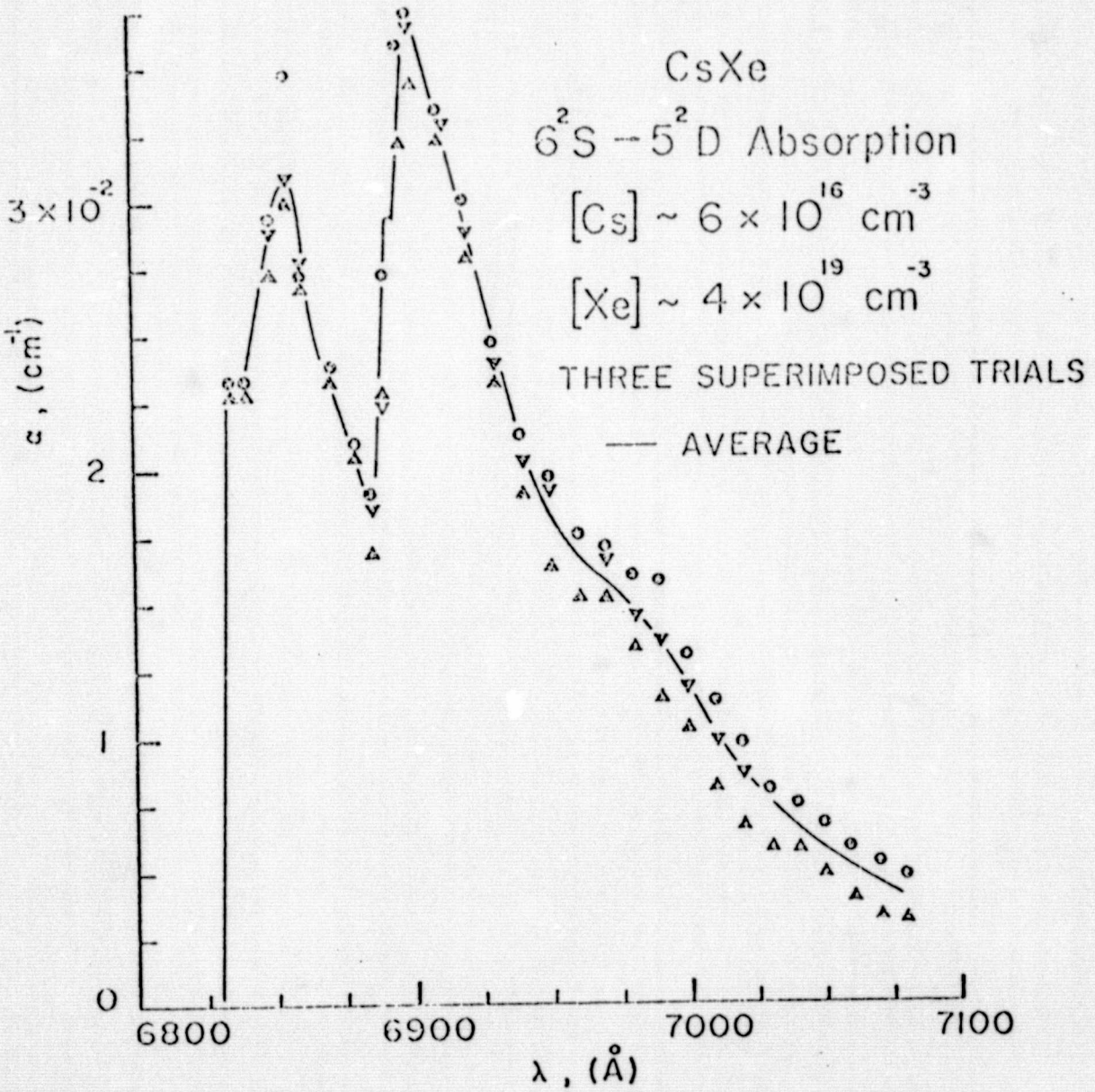

Fig. 7. Three superimposed trials of the absorption coefficient, α, versus λ for [Xe] $\sim 4 \cdot 10^{19}$ cm^{-3} and [Cs] $\sim 6.3 \cdot 10^{16}$ cm^{-3}.

III. EXPERIMENTAL RESULTS AND DISCUSSION

A. Absorption and Fluorescence Spectra Of The $(Cs[5^2D]Xe)^*$ Molecule

Figures 8-10 display the Cesium density dependence of the absorption coefficient for the Xenon-perturbed $Cs(6^2S \rightarrow 5^2D)$ transitions. These measurements were conducted for three constant Xenon densities in the range $[Xe] \sim 3\text{-}5 \cdot 10^{19}$ cm^{-3} (1-2 atmospheres at room temperature). An unusual feature of these absorption profiles is a "shoulder" situated to the blue side of both the 6849 and 6895 Å lines, the onset of which is very sudden and is roughly independent of Cesium density. (This feature is particularly noticeable at the lower Xenon densities). The energy separation between the shoulder and atomic line center for both of these transitions is about 25 - 30 cm^{-1}. Thus, this observed blue shoulder may be interpreted as due to transitions of weakly bound ground state CsXe molecules to the 5^2D Cesium atomic states. That is:

$$CsXe + h\nu \rightarrow Cs^* + Xe \ . \qquad (2)$$

Absorption characteristics similar to those observed here have been recently reported for the heteronuclear rare gas molecules (such as XeAr) by Freeman and co-workers.[18] It is interesting that they have interpreted their results in the same way as presented here. This

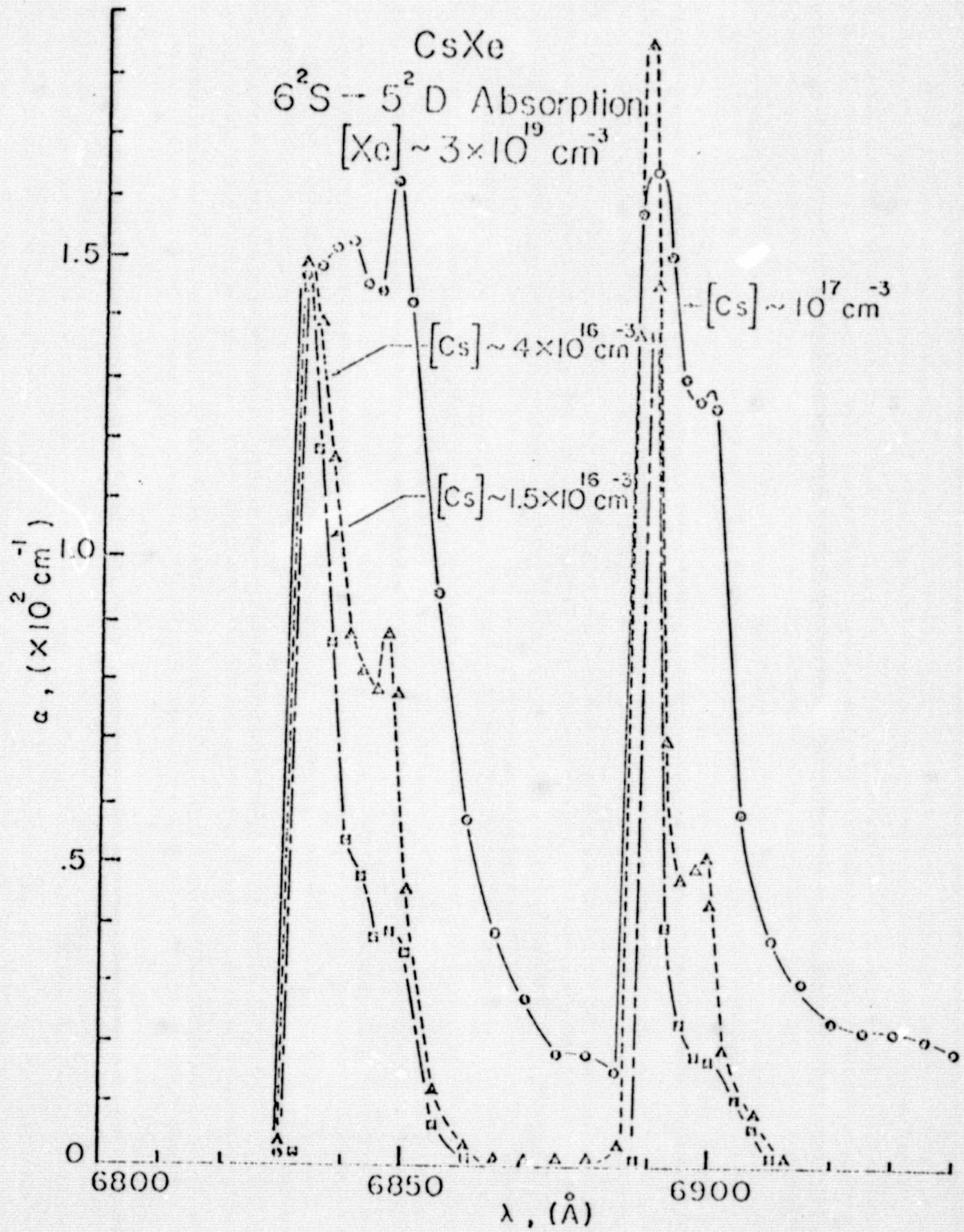

Fig. 3. Cs($6^2S \rightarrow 5^2D$) absorption spectra for various Cesium densities and [Xe] $\sim 3 \cdot 10^{19}$ cm^{-3}.

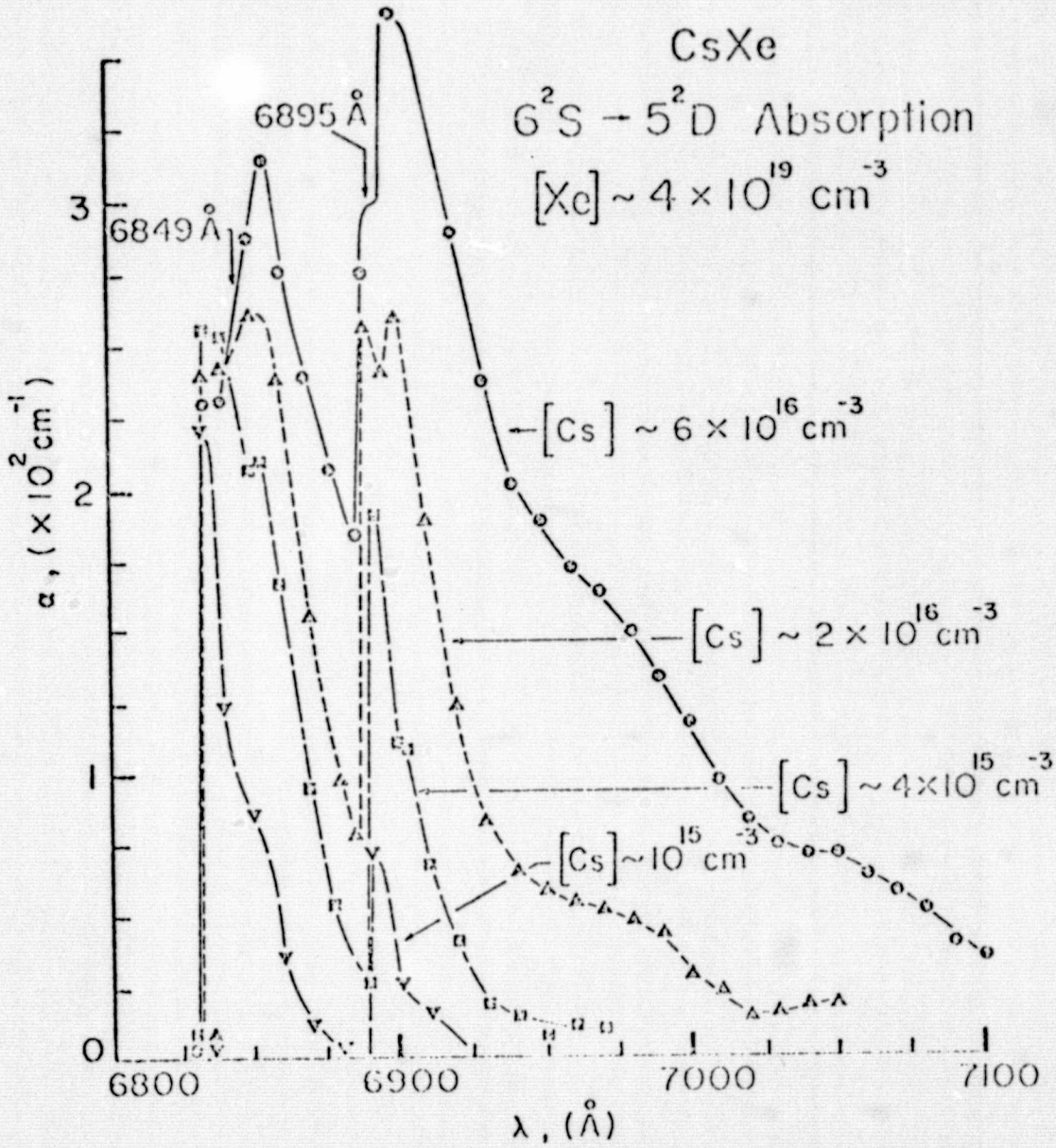

Fig. 9. Cesium density dependence of the $6^2S \cdot 5^2D$ absorption coefficient for $[Xe] \sim 4 \cdot 10^{19}\ cm^{-3}$.

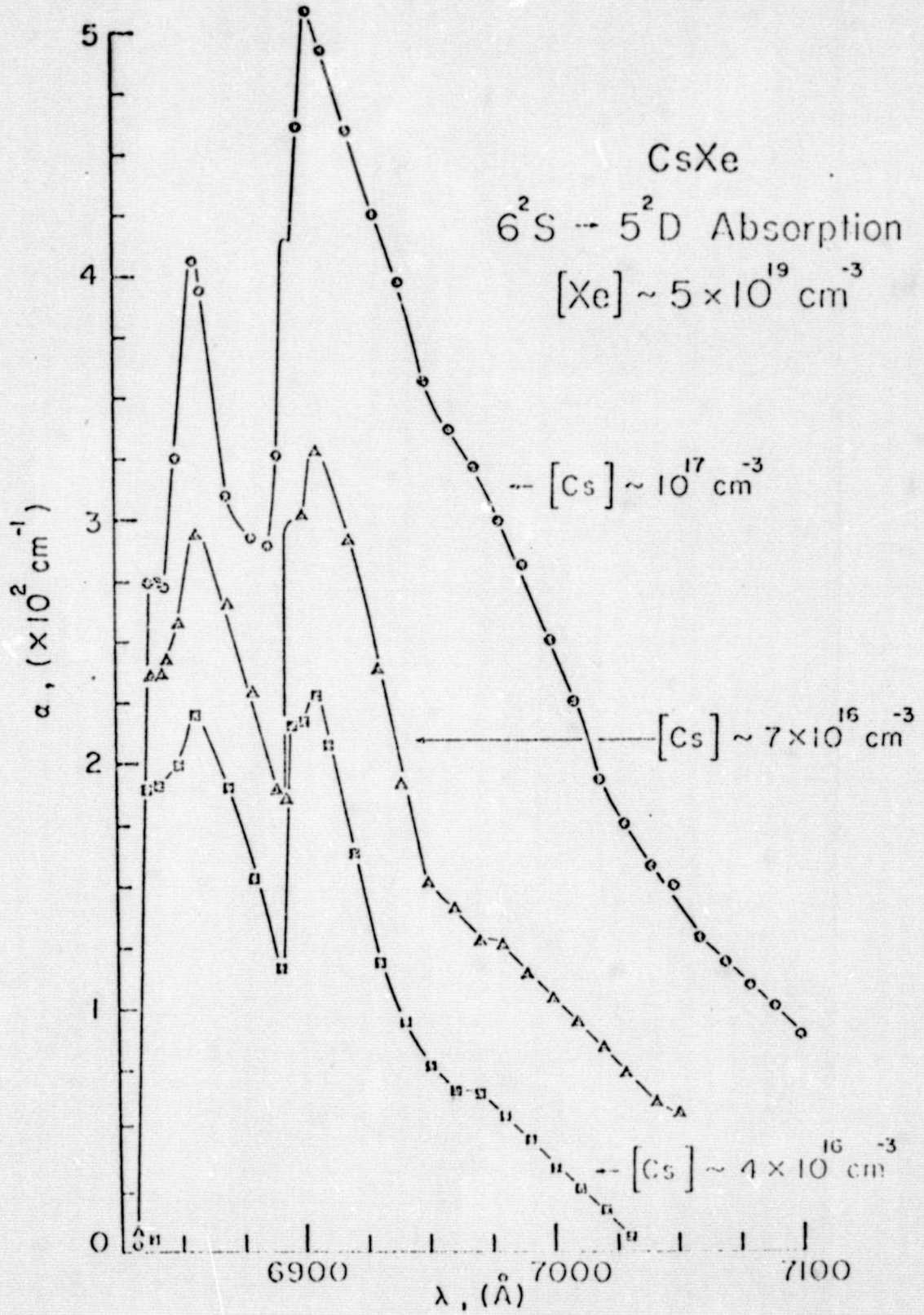

Fig. 10. Absorption spectra ($6^2S \rightarrow 5^2D$) for $[Xe] \sim 5 \cdot 10^{19}$ cm^{-3} (2 atm. at room temperature) showing noticeable growth of the molecular continuum absorption as [Cs] increases.

is also consistent with the work of Hedges, Drummond and Gallagher[11] who have experimentally determined the binding of the CsXe molecule to be $< 100\ cm^{-1}$. Therefore, these molecular → excited atomic transitions originate at the lowest vibrational states of the weakly bound CsXe molecule. This accounts for the rapid onset of absorption as the 6849 Å transition is approached from the blue side.

At low Xenon densities, absorption at the forbidden atomic lines grows rapidly with increasing Cesium pressure and eventually dominates the spectra. However, the emergence of the so-called "forbidden" red satellite becomes obvious at the higher Xenon densities. Such satellites have been reported for several alkali-rare gas mixtures[12-15] but, to our knowledge, this is the first report of such satellites on the $6^2S \rightarrow 5^2D$ absorptive transitions in CsXe. These satellites are analogous to those found previously for allowed S → P transitions of the rare gas perturbed alkalis[19] and peak $\sim 4 - 5$ Å to the red side of the forbidden atomic transitions. Although there is debate as to the origin of these satellites, it is generally thought that they arise when the energy difference between the upper and lower molecular potential curves is independent of radius [i.e., $\frac{d}{dr}\{V_u(R) - V_L(R)\} = 0$].[10] This condition leads to a singularity in the fluorescence spectrum which is subsequently smoothed by Doppler effects. At the highest Xenon densities investigated in these experiments, the red satellites are the most conspicuous features of the spectra.

Xenon pressure dependent absorption spectra for the $6^2S \rightarrow 5^2D$ lines are shown in Fig. 11 for a fixed Cs density. A broad molecular continuum associated with the forbidden atomic transitions emerges at higher Xenon densities, extending 200 - 300 Å to the red side of the forbidden atomic transition. This spectral feature is associated with transitions to $[CsXe]^*$ and is the most important feature of these spectra relative to possible laser applications.

Atomic line absorption on the "forbidden" $6^2S \rightarrow 5^2D$ transitions in the presence of Xenon is collisionally induced.[6,20,21] Ordinarily, the $^2S \rightarrow {}^2D$ electric quadrapole transition probability is insignificant. However, collisions of ground state Cesium and Xenon atoms cause the overlap integral of the ground and excited state wave functions (i.e., electric dipole moment) to assume a non-zero value. Thus, optical transitions between the Cesium 6^2S and 5^2D states become allowed and are characterized by a transition probability A which is directly proportional to the Xenon density. That is,

$$A = k_o [Xe] \quad , \tag{3}$$

where k_o is the collisionally induced emission coefficient in cm^3 -sec^{-1}, A is the $6^2S \rightarrow 5^2D$ transition probability in sec^{-1} and

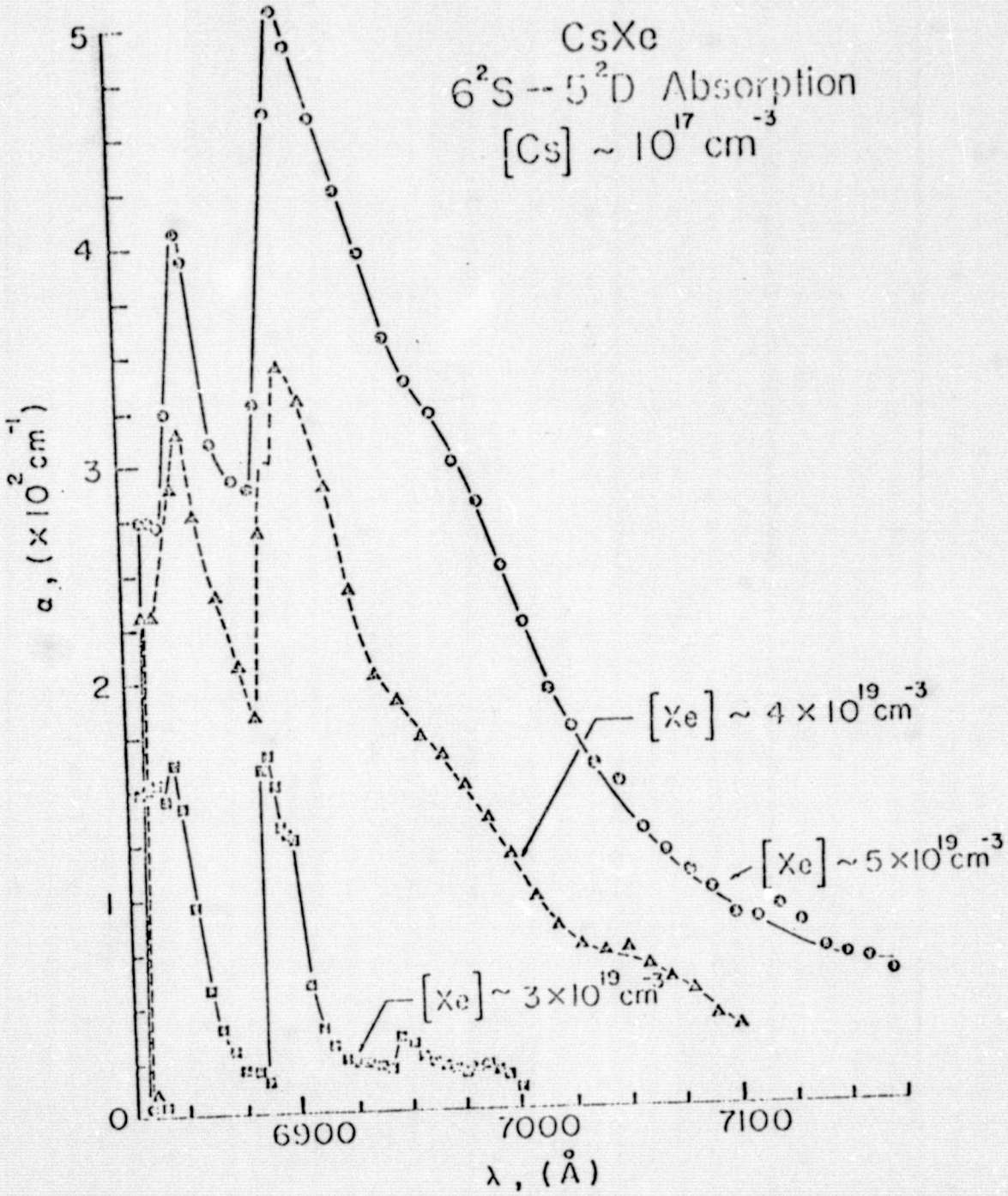

Fig. 11. Xenon density dependence of the $6^2S - 5^2D$ atomic-molecular absorption spectrum for $[Cs] \sim 10^{17}\ cm^{-3}$.

[Xe] is the Xenon density expressed in cm^{-3}. To determine k_o from the experimental absorption data, the absorption equation is solved to obtain an expression for the atomic spontaneous radiative rate. That is:

$$\left|\alpha(\lambda)\right| = \frac{\lambda^2}{8\pi} \frac{g_U}{g_L} N_L \; g(\lambda) \; A \qquad (4)$$

may be rewritten as

$$A = \frac{\alpha}{[Cs]} \frac{8\pi}{\lambda^2} \frac{g_L}{g_U} \Delta\nu \qquad (5)$$

where $g_{L,U}$ are the degeneracies of the ground and excited atomic states, respectively, and the absorption lineshape has been related to the inverse of the lineshape's half-width, $\Delta\nu$. Using Eq. (3), relation (5) becomes:

$$k_o \; (cm^3 - sec^{-1}) = \frac{8\pi}{\lambda^2} \frac{g_L}{g_U} \left(\frac{|\alpha|}{[Xe]}\right)\left(\frac{\Delta\nu}{[Cs]}\right). \qquad (6)$$

Figure 12 depicts the linear variation of α versus Xenon density ([Cs] $\sim 10^{17}$ cm^{-3}), as derived from Fig.11, for the 6849 Å transition. The slope of this line is associated with the collision induced emission coefficient which (from Eq. (6)) was determined to be $k_o \sim 3 \cdot 10^{-17}$ cm^3 - sec^{-1}, ($5^2D_{5/2} \rightarrow 6^2S_{1/2}$), where $\Delta\lambda$ was estimated from the low [Xe] absorption spectra to be approximately 20 Å. Setting [Xe] = 5×10^{19} cm^{-3}, collisional lifetimes on the order of 0.7 msec are obtained for this state. Clearly, then, loss of the 5^2D excited state population due to collisionally induced radiative transitions to ground is negligible when compared to radiative losses to the 6^2P levels ($\tau \sim$ nsec).[22] A similar analysis for the Cs($5^2D_{3/2} \rightarrow 6^2S_{1/2}$) transition was not carried out since the absorption coefficient at 6895 Å shown in Fig. 11 includes a contribution due to the red wing of the 6849 Å line. This additional absorption causes the 6895 Å absorption coefficient to deviate significantly from linearity at the higher Xenon pressures. Also, applying the absorption equation to far red wing absorption, the spontaneous radiative lifetime, τ, for the $(Cs[5^2D]Xe)^*$ excimer was determined to be in the microsecond regime.

The near red wing absorption coefficient of the 6849 and 6895 Å forbidden lines varies approximately linearly with the product of the Cesium and Xenon densities as shown in Figs. 13-15 for several Xenon pressures. Here the absorption coefficient spectra, normalized to both [Cs] and [Xe], overlap for $6900 \lesssim \lambda \lesssim 6950$.

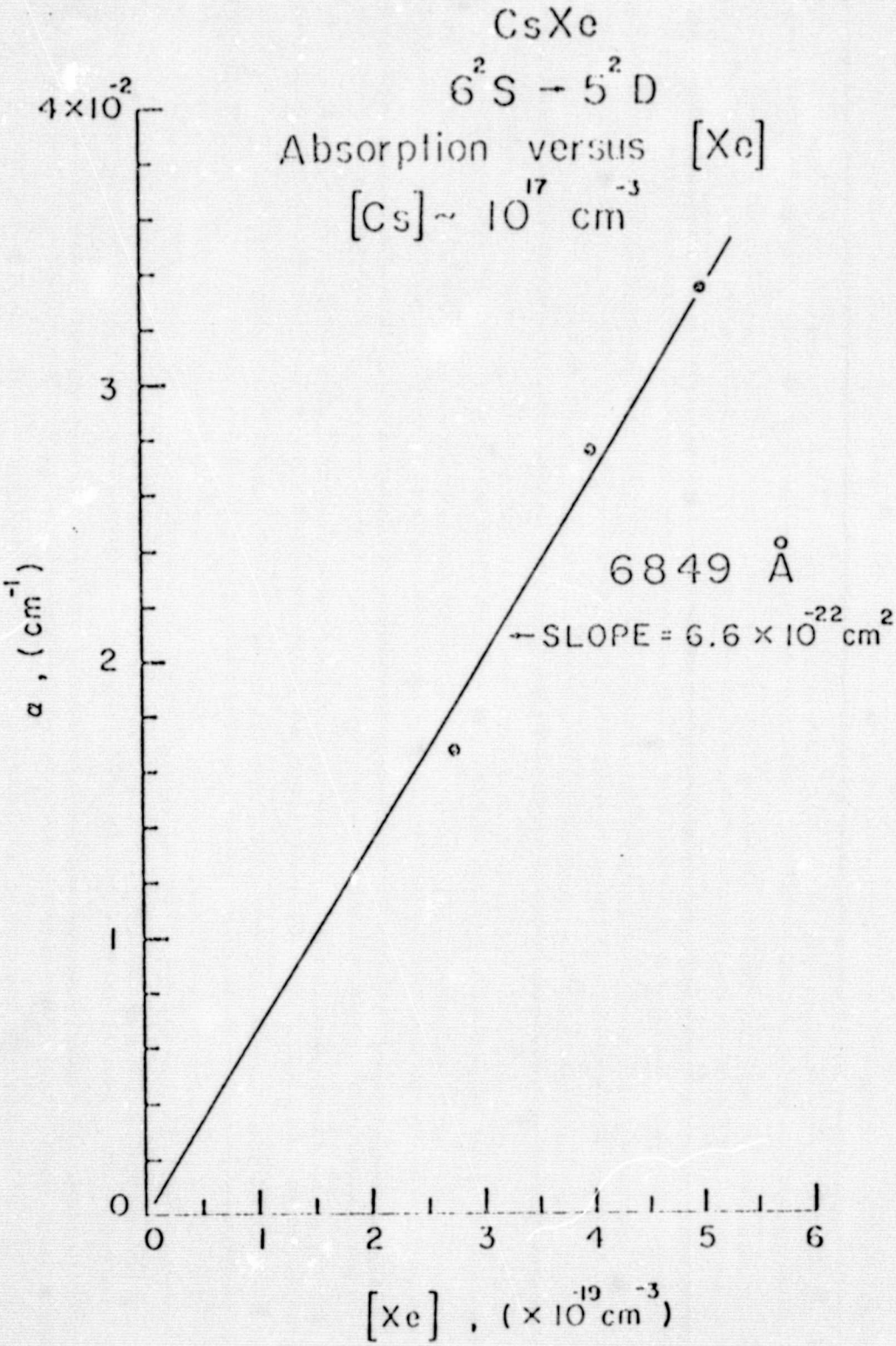

Fig. 12. Plot showing the linear dependence of the absorption coefficient at 6849 Å on Xenon density.

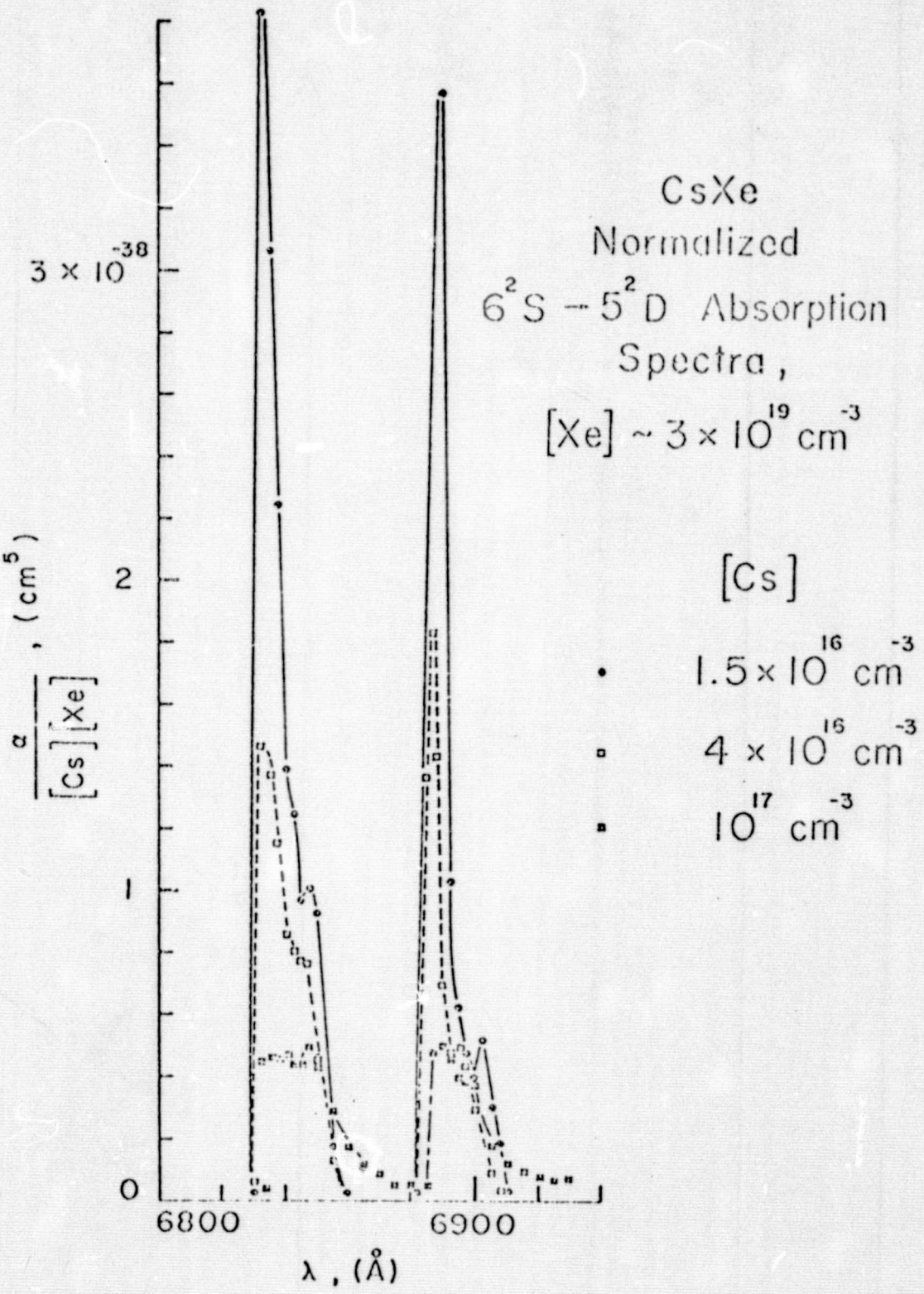

Fig. 13. Normalization of $6^2S \rightarrow 5^2D$ absorption spectra to [Cs][Xe] for [Xe] $\sim 3 \cdot 10^{19}$ cm^{-3}. Note the overlap of the profiles in the vicinity of 6849 and 6895 Å.

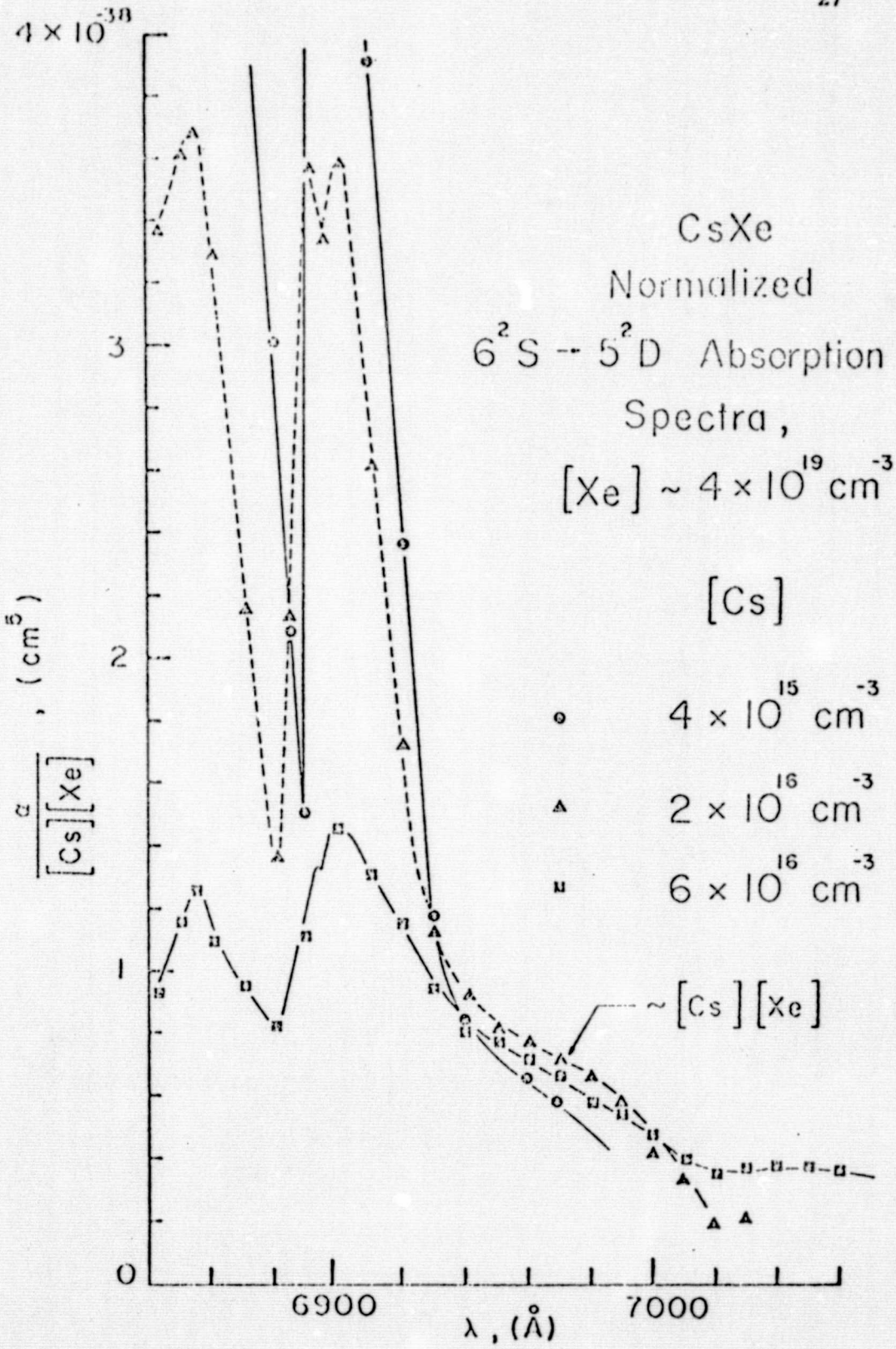

Fig. 14. Similar normalization plot for [Xe] ~ $4 \cdot 10^{19}$ cm^{-3}. For the wavelength region $6940 \leq \lambda \leq 6980$, the normalized profiles overlap.

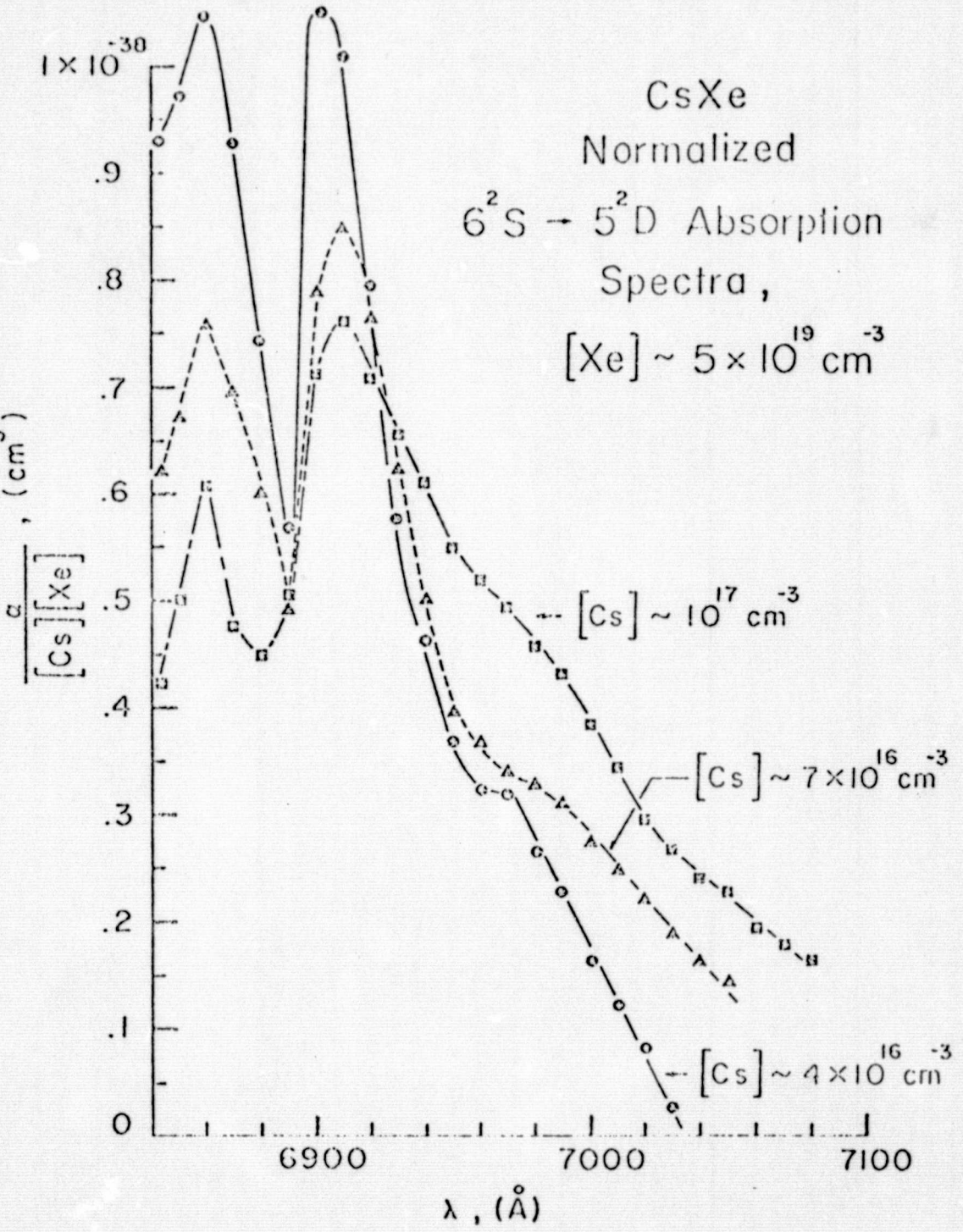

Fig. 15. Normalized absorption profiles for [Xe] ~ $5 \cdot 10^{19}$ cm^{-3} showing deviation from linearity in the red wing. This is due to increasing [CsXe] at R_o (see text).

This behavior is typical of unbound molecular absorption.[23] However, at the highest Cesium and Xenon densities studied (cf. Fig. 15), the far red wing absorption deviates significantly from linearity. This suggests that these far wing transitions are occurring between the $(CsXe)^*$ excited molecular state and a strongly repulsive portion of the ground state. This conclusion is best illustrated by Fig. 16 where an energy diagram for a typical ground molecular state is shown. The CsXe ground state density at an interatomic radius, R_o, is given by:

$$[CsXe](R_o) \sim 4\pi R_o^2 \, dR \, [Cs][Xe] \exp\left\{-\frac{\Delta E}{kT}\right\} . \quad (7)$$

Therefore, any temperature rise in the system will initiate a significant increase in [CsXe] at R_o through the Boltzmann factor and by directly affecting the [Cs] term. Note also that [CsXe] $\sim$ [Xe]; hence, the deviation of $\alpha/[Cs][Xe]$ from linearity is more pronounced at the higher Xenon densities. Finally, since the absorption coefficient is directly proportional to [CsXe], we conclude that large changes in $\frac{\alpha}{[Cs]\,[Xe]}$ for increasing Cesium densities reflect the fact that a rapidly growing number of CsXe molecules are available at R_o to undergo absorptive transitions. We infer from the preceding arguments that these far wing optical transitions originate at a strongly repulsive portion of the ground state.

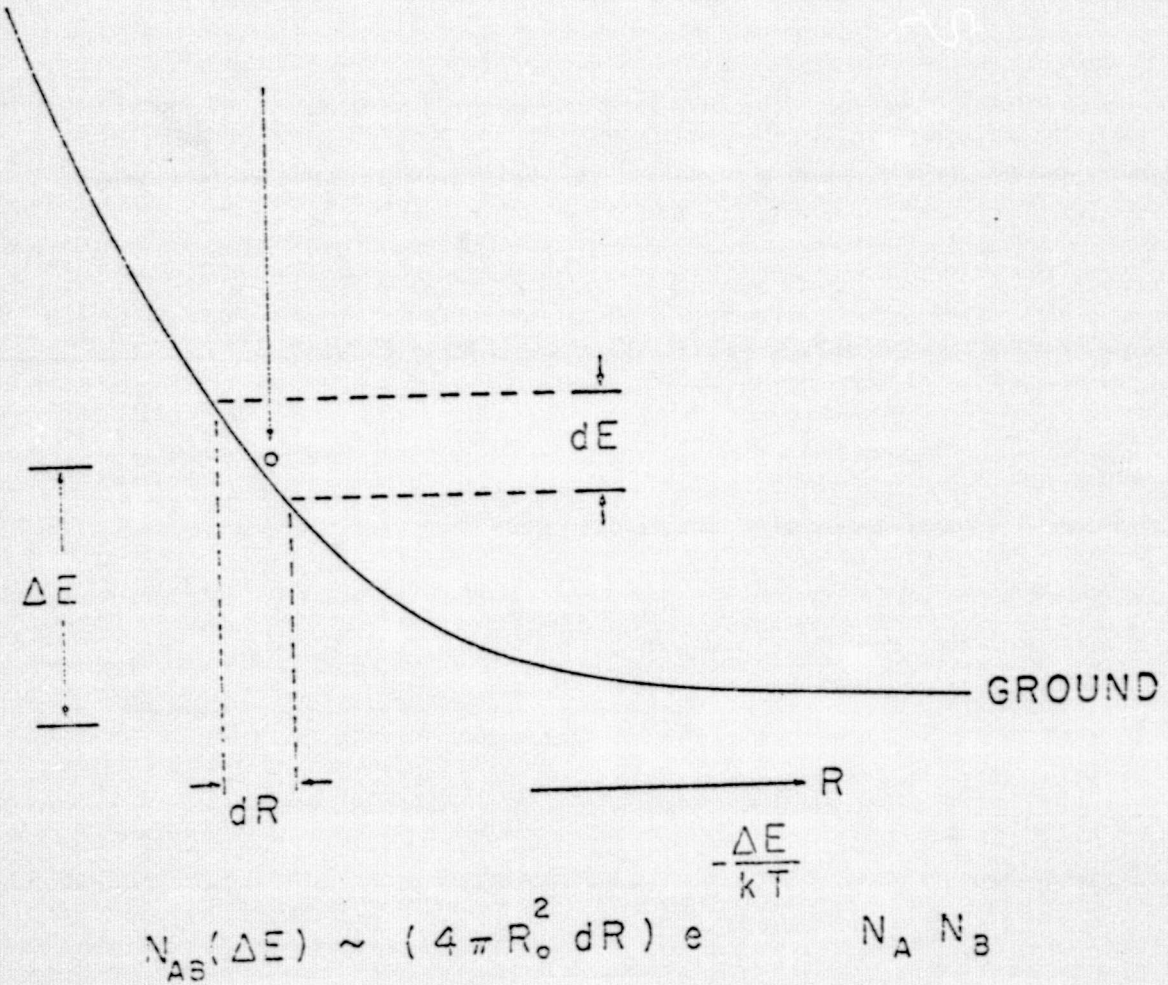

Fig. 16. Ground state potential for the unstable molecule AB. Also given is the relation for the molecular density at the interatomic radius, R_o.

The spectrally-resolved flashlamp-pumped fluorescence and absorption spectra for $(Cs[5^2D]Xe)^*$ molecules is shown in Fig. 17 ($[Xe] \sim 5 \cdot 10^{19}$ cm^{-3}, $[Cs] \sim 10^{17}$ cm^{-3}). Clearly, peak molecular emission does not coincide in wavelength with maximum absorption. There are several interrelated explanations for this phenomenon. First, at the Cesium densities employed in this experiment, the gaseous medium is not optically thin; hence radiation trapping in the near wing of the atomic lines is significant. Also, as mentioned previously, due to the repulsive ground state, absorption occurs primarily at large interatomic radii compared to the excimer emission. To estimate the contribution of these effects to the emission profile, we utilize the arguments of Phelps[10] to calculate the excimer fluorescence profile using previously given absorption data and the theoretical CsXe potential energy curves of Pascale and Vandeplanque.[24] From Phelps' semi-classical analysis, the emission spectrum $I(\lambda)$ may be obtained from the known absorption spectrum, $\alpha(\lambda)$, by the relation:[10]

$$I(\lambda) = \alpha(\lambda) \frac{hc}{\lambda^3} \frac{N_U}{N_L} \exp\left\{\frac{|\Delta V_U| + |\Delta V_L|}{kT}\right\} \quad (8)$$

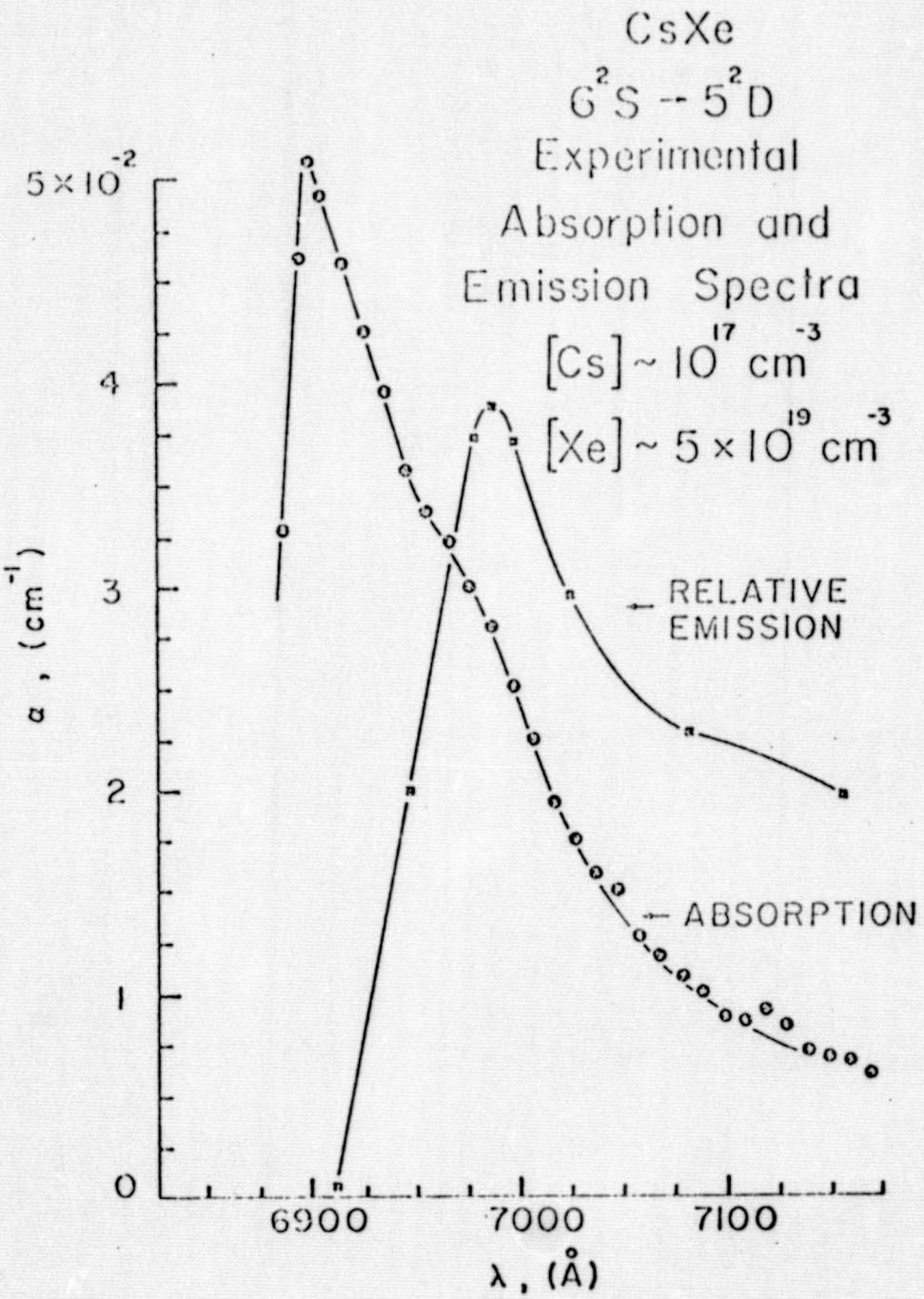

Fig. 17. Plot of absorption coefficient and relative emission spectra ($6^2S \rightarrow 5^2D$) for $[Cs] \sim 10^{17}\ cm^{-3}$ and $[Xe] \sim 5 \cdot 10^{19}\ cm^{-3}$.

where N_U and N_L are the upper and lower state population densities, respectively, and ΔV_U, ΔV_L and λ are defined by the equations:

$$\Delta V_U(R_o) = V_U(\infty) - V_U(R_o) \quad ,$$
$$\Delta V_L(R_o) = V_L(R_o) - V_L(\infty) = V_L(R_o) \qquad (9)$$

and

$$V_U(R_o) - V_L(R_o) = \frac{hc}{\lambda} \quad .$$

Once $I(\lambda)$ has been calculated from $\alpha(\lambda)$ using the potential energy curves, we must account for the effect of trapping of the fluorescence (cf. Fig. 18). The spectrum $I(\lambda)$ (given by Eq. (8)) is emitted from the differential tube length dx and is located a distance x from the end of the absorption tube. Therefore, the actual fluorescence spectrum emerging from the tube is given by:

$$I'(\lambda) = \int_{x=0}^{L} I(\lambda) \exp\left\{-\alpha(\lambda)x\right\} dx \qquad (10)$$

where L = absorption tube length = 15.7 cm. Equations (8) and (10)

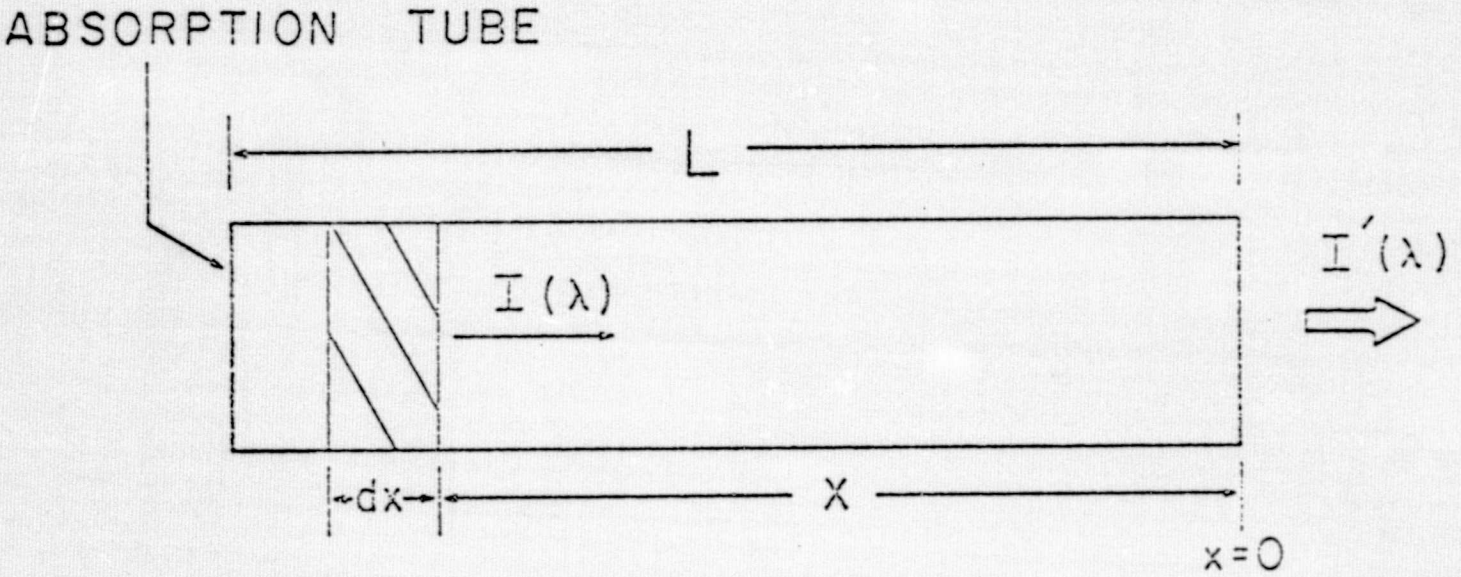

$$I'(\lambda) = \int I(\lambda) \exp\left\{-\alpha(\lambda)x\right\} dx$$

Fig. 18. Schematic of absorption tube including the relation used to account for radiation trapping of the excimer fluorescence.

have been evaluated using absorption data given previously and the results are displayed in Fig. 19. Also shown are the experimentally measured $6^2S \rightarrow 5^2D$ absorption and emission spectra ([Cs] $\sim 10^{17}$ cm^{-3}, [Xe] $\sim 5 \cdot 10^{19}$ cm^{-3}). It is clear that although the emission spectrum $I'(\lambda)$ is slightly shifted to the red of peak absorption, the theoretical and experimental fluorescence maxima do not coincide. This may be explained through careful scrutiny of the absorption and emission processes (see Fig. 20).

The molecular absorption coefficient is proportional to the product of the ground (lower) state density and the quantum-mechanical matrix element describing the overlap of the lower and upper energy state wavefunctions. This matrix element is defined by:

$$\langle U | \mu | L \rangle = \langle \psi_U | \mu | \psi_L \rangle = \int \psi_U^* \mu \psi_L \, d\tau \qquad (11)$$

where:

ψ_L is the lower state wavefunction,

ψ_U is the upper state wavefunction,

μ is the dipole moment of the transition

and $d\tau$ is a differential element of real space.

Hence, we can roughly express the absorption coefficient $\alpha(\lambda)$ as:

$$\alpha(\lambda) \sim N_L(E) \langle U | \mu | L \rangle \qquad (12)$$

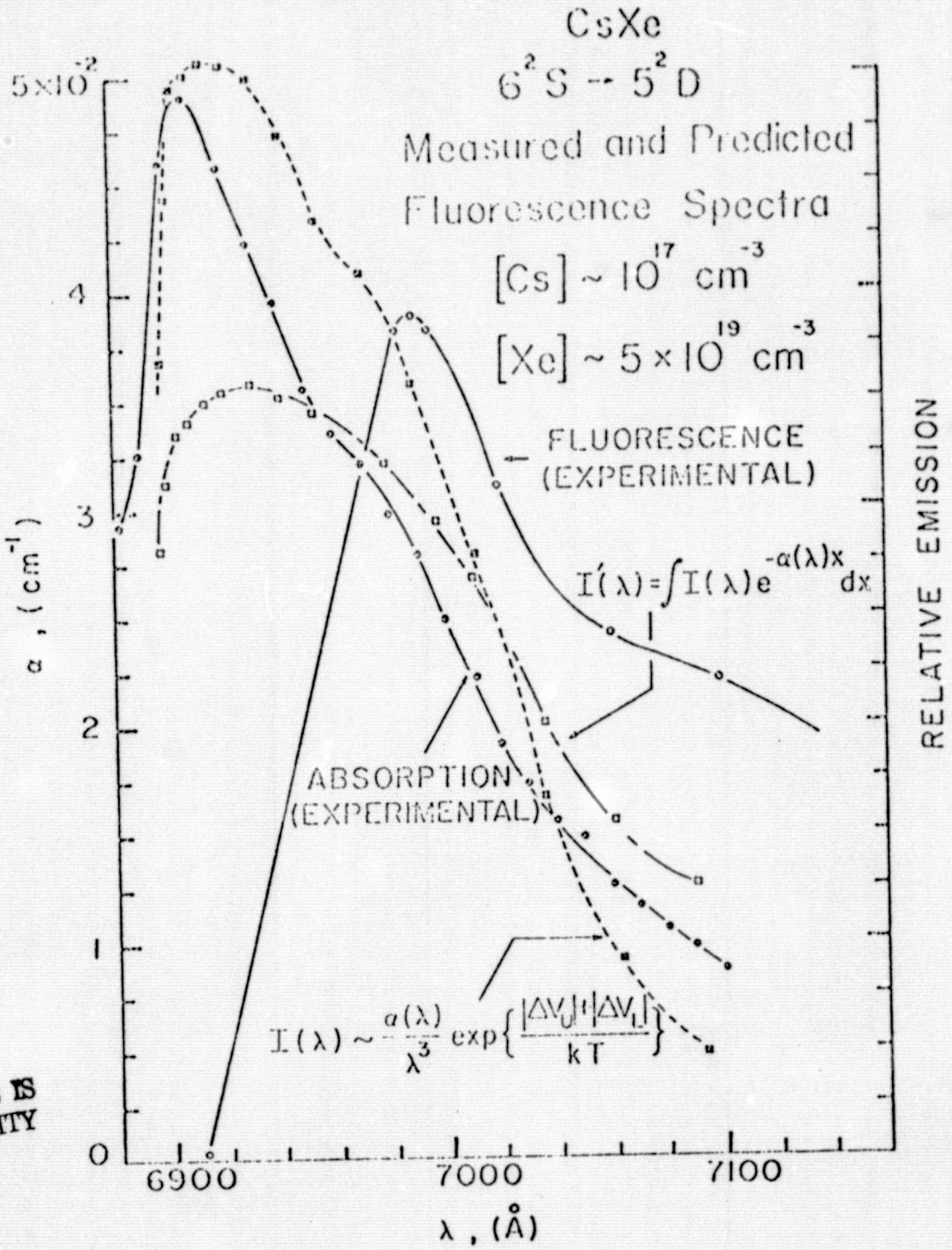

Fig. 19. Graph displaying: a) experimental absorption spectrum, b) experimental emission spectrum, c) theoretical emission, I(λ), calculated using Phelps' analysis[10] in conjunction with Pascale and Vandeplanque's potential curves and d) $I(\lambda)$ corrected for radiation trapping effects for the $(Cs[5^2D]Xe)^*$ excimer.

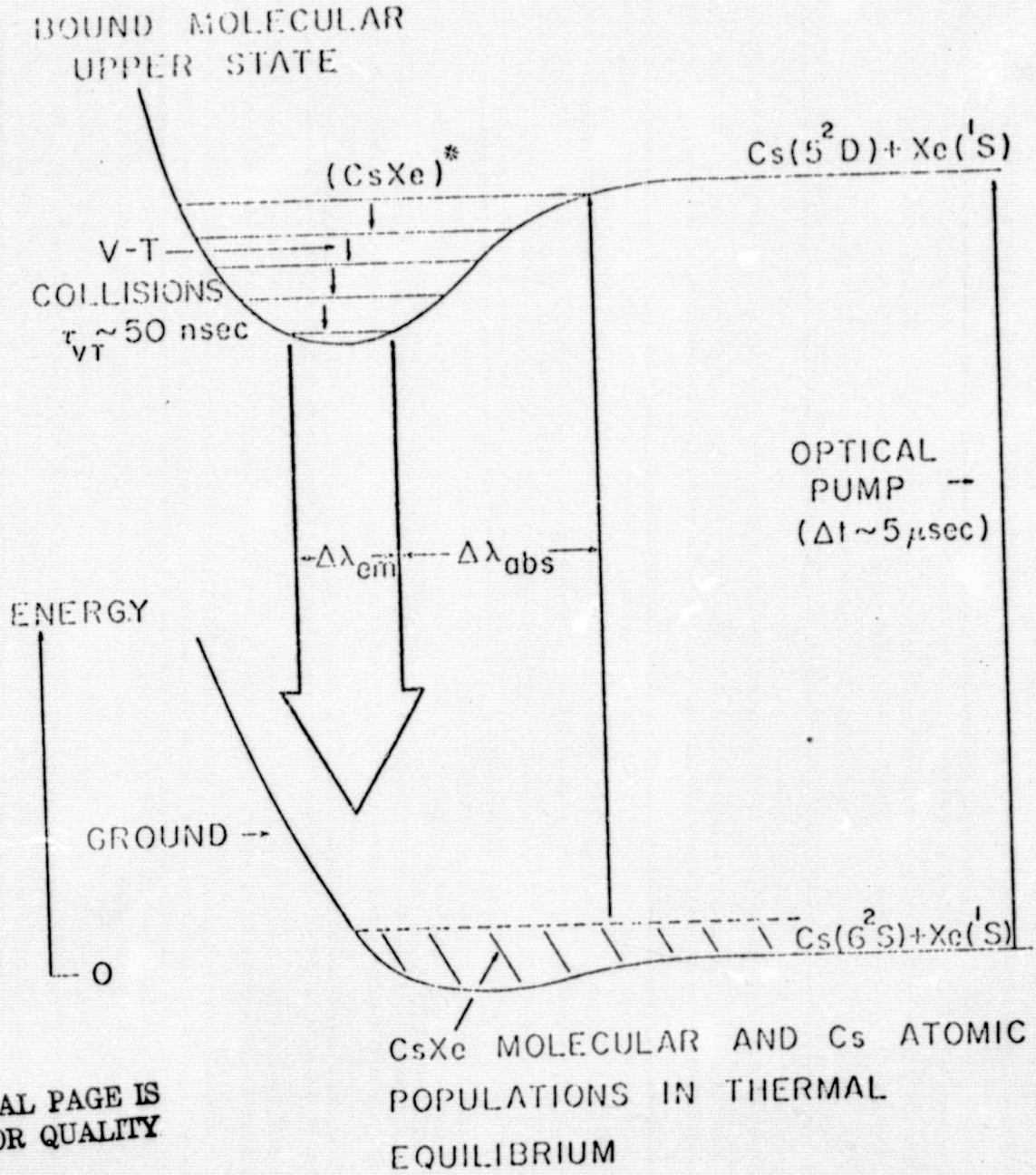

Fig. 20. Partial energy level diagram for the $(Cs[5^2D]Xe)^*$ excimer showing processes responsible for the observed absorption and fluorescence spectra.

where again $E_U - E_L = \frac{hc}{\lambda}$. Obviously, the matrix element varies depending on the upper and lower states of interest. Secondly, please note that since the wavefunction product is integrated over real space, then the magnitude of this matrix element is inherently linked to the volume of real space occupied by the upper state vibrational level where the absorptive transition terminates (which, incidentally, is proportional to the density of states available to a CsXe molecule absorbing a photon). Also, the absorption measurements in these experiments were conducted under quasi-continuous conditions, insuring that the molecular and atomic ground state populations were in equilibrium. We conclude, then, from Eq. (12) that absorption under these conditions favors high lying vibrational levels of the upper molecular state, i.e., the largest number of available states for the transitions. Hence, the majority of the absorption occurs at wavelengths in close proximity to, and to the red side of, the atomic line.

In contrast, emission measurements were carried out over short time scales (i.e., non-equilibrium conditions). Of particular significance are vibrational-translational(V-T) collisions which deactivate vibrationally excited $(CsXe)^*$ molecules. That is:

$$\left[CsXe(v)\right]^* + Xe \rightarrow \left[CsXe(v')\right]^* + Xe + \Delta E \qquad (13)$$

where $v > v'$. The V-T deactivation rate may be estimated from known

V-T energy exchange probabilities[25,26] for lighter molecules such as N_2 and CO. For [Xe] $\sim 10^{20}$ cm^{-3}, the estimated V-T de-excitation rate is $\sim 2 \cdot 10^7$ sec^{-1}, yielding vibrational lifetimes of $\sim$ 50 - 100 nsec, which is expected to be a generous upper limit for $(CsXe)^*$. Clearly, these lifetimes are small compared to the spontaneous radiative lifetime of the excimer ($\sim$ μsec). Therefore, a vibrationally excited $(CsXe)^*$ molecule that is newly formed by the optical pump will rapidly undergo vibrational de-excitation collisions, causing the excited molecular population to be concentrated in low vibrational number quantum states. As a result, the bulk of the excited molecular emission takes place from low-lying vibrational states to ground and thus is representative of the distribution of occupied states within the $(CsXe)^*$ molecular well.

In summary, then, the equilibrium absorption process emphasizes transitions from ground to high-lying $(CsXe)^*$ vibrational states, requiring the absorption of near wing photons; whereas, since the V-T de-excitation lifetime is short compared to the $(CsXe)^*$ state's spontaneous lifetime, then newly-formed $(CsXe)^*$ molecules tend to vibrationally collapse to low lying vibrational levels and subsequently radiate, yielding far wing photons. Under the conditions of our experiment, therefore, one would expect the emission spectrum to be relatively narrow and displaced to wavelengths to the red of peak absorption.

Figures 21 and 22 display these $(CsXe)^* 5^2D$ emission profiles as a function of Cesium and Xenon density. Note that for a fixed Cesium density, increasing the Xenon pressure modifies the spectrum shape markedly due to equilibration of the molecular well (cf. Fig. 21). Yet, as expected, increasing the Cesium density for constant Xenon pressure has little effect on the emission spectrum shape.

B. Spectra For The $(Cs[7^2S]Xe)^*$ Molecular State

The absorption and relative emission profiles for the $(Cs[7^2S]Xe)^*$ molecular state are shown in Fig. 23. In this case, dominant absorption occurs at $\sim$ 5723 Å, over 300 Å from the atomic transition at 5395 Å. This point, in conjunction with the fact that the far wing absorption closely follows the measured fluorescence, indicates that we are observing transitions connecting the bottom of the $(CsXe)^*$ molecular well with ground. In contrast to the 5^2D states, the 7^2S excimer far wing absorption profiles do not change significantly with varying Cesium density (i.e., temperature) as shown in Fig. 24. When these spectra are normalized to the Cesium density, they overlap within $\sim$ 20%, as shown in Fig. 25. (This error becomes noticeable only at low Cesium densities and arises due to the difficulty in accurately measuring small changes in percentage absorption). It is for this reason that we were unable to measure 5723 Å absorption at Xenon densities lower than $5 \cdot 10^{19}$ cm^{-3}.

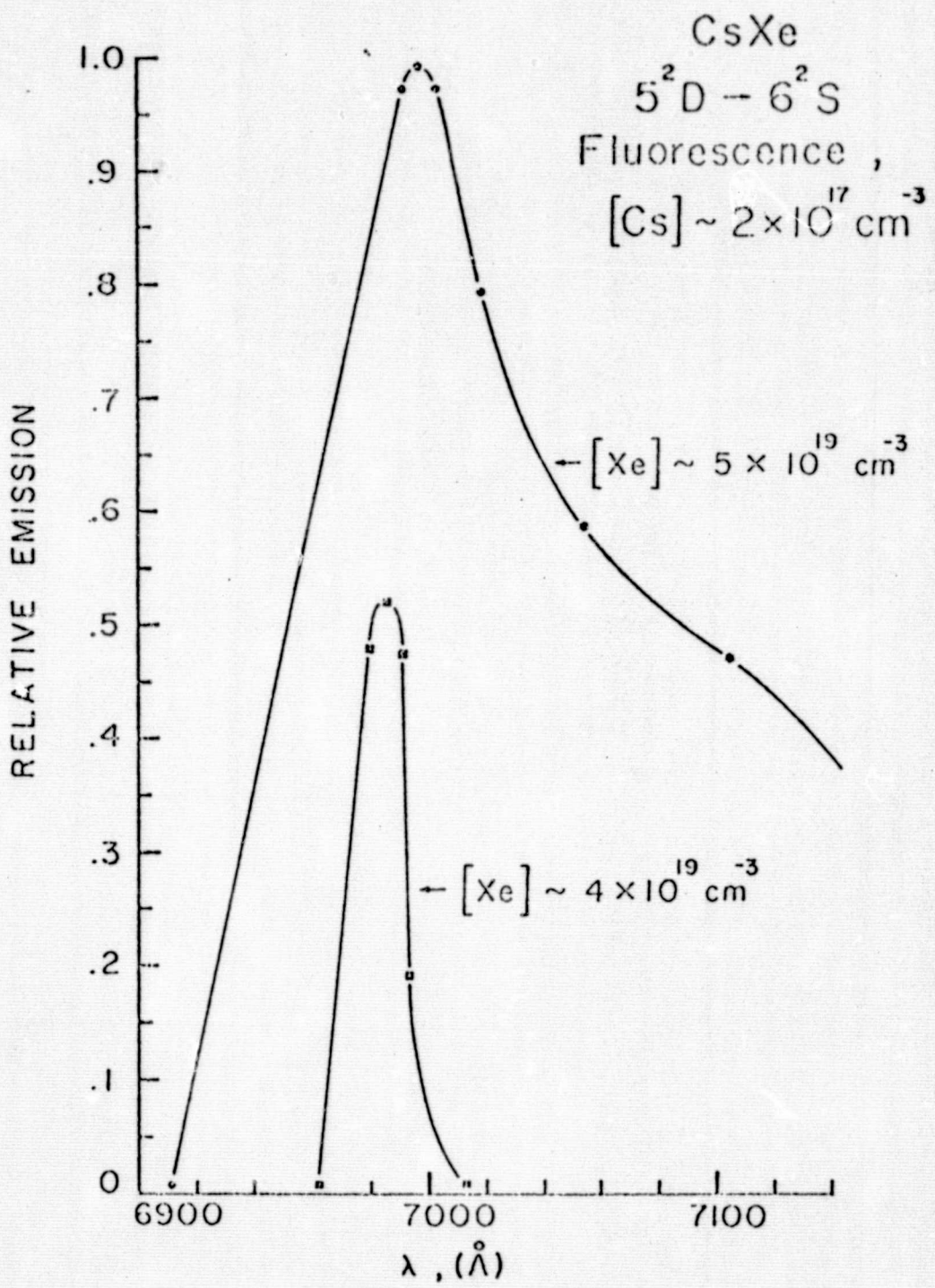

Fig. 21. Xenon pressure dependence of the $(Cs[5^2D]Xe)^*$ excimer fluorescence.

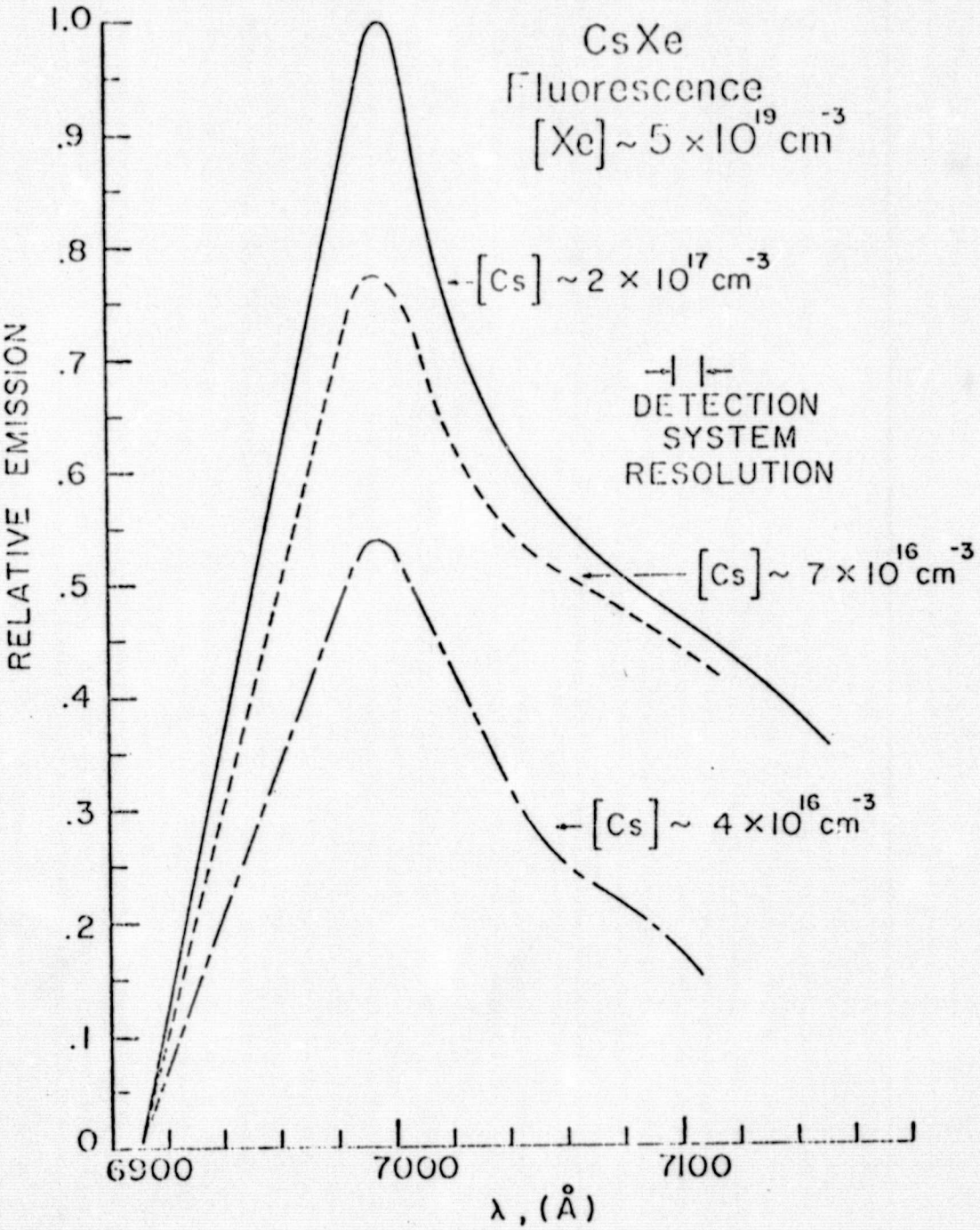

Fig. 22. Cesium density dependence of the $(Cs[5^2D]Xe)^*$ excimer fluorescence for [Xe] ≈ $5 \cdot 10^{19}$ cm^{-3}.

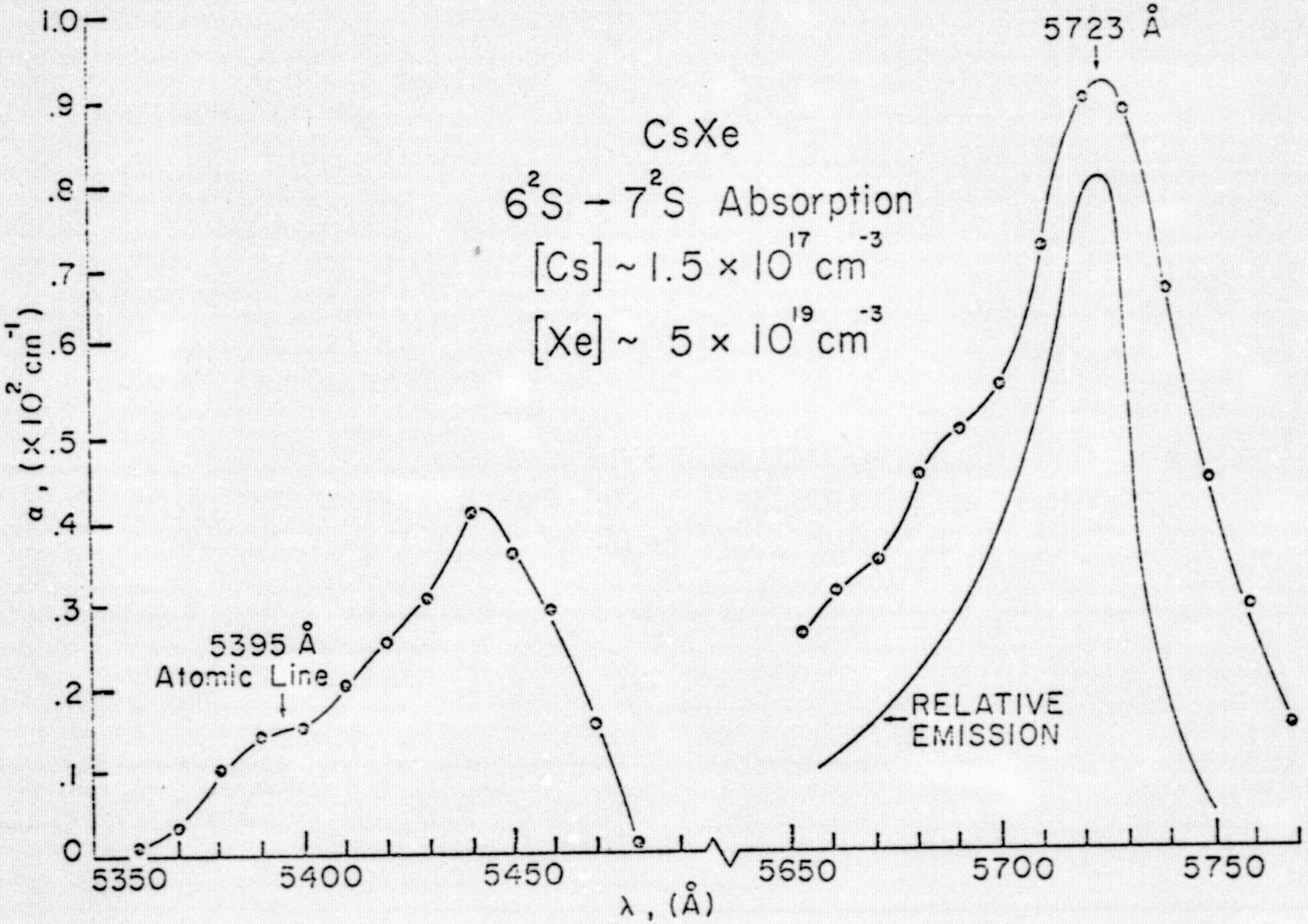

Fig. 23. Absorption and relative emission spectra of the $Cs^*(7^2S)$ - $(Cs[7^2S]Xe)^*$ atomic-molecular system.

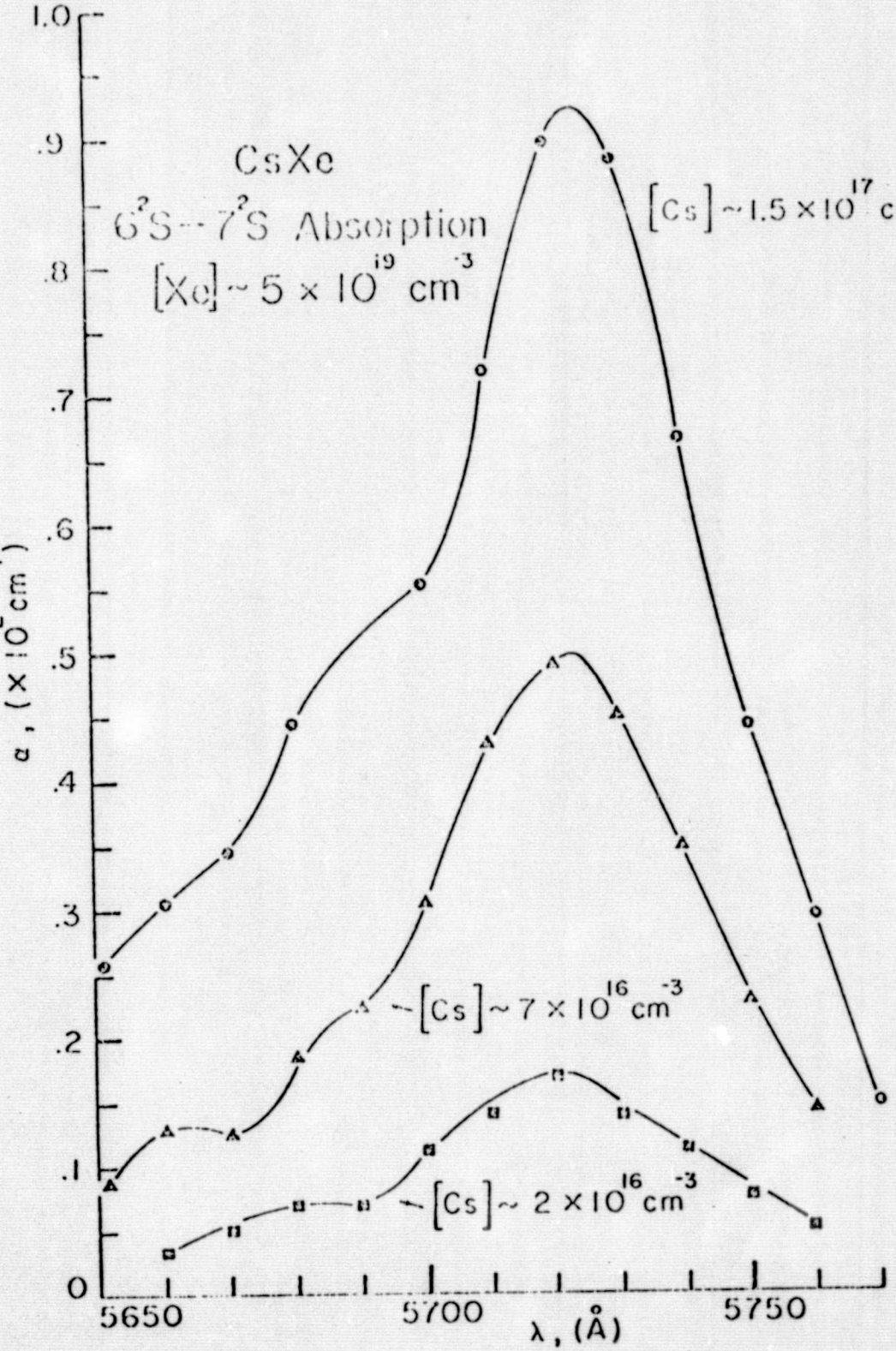

Fig. 24. Variation of $(Cs[7^2S]Xe)^*$ absorption spectra with increasing Cesium pressure, $[Xe] \sim 5 \cdot 10^{19}$ cm^{-3}.

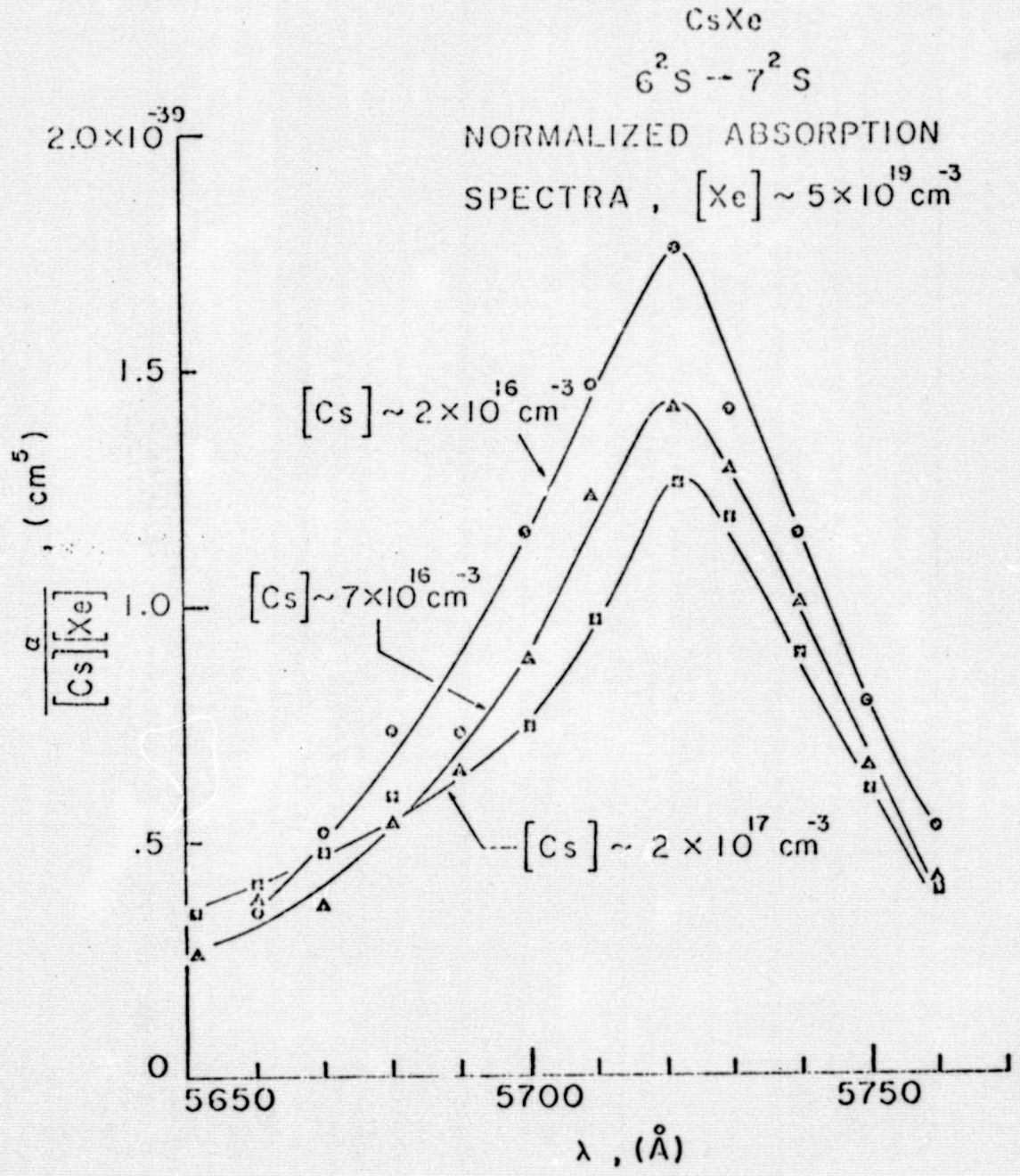

Fig. 25. Normalized $(Cs[7^2S]Xe)^*$ absorption profiles for [Xe] ~ $5 \cdot 10^{19}$ cm^{-3}. These spectra overlap within 20%.

Therefore, normalization of these profiles to the Cesium density suggests that the 5723 Å - centered molecular band terminates on a portion of the ground state that is not strongly repulsive. Combining the conclusions implied by the data of Figs. 24 and 25, the $(CsXe)^*$ molecular well depth is approximately 1062 cm^{-1} = .132 eV. Fluorescence data, similar to that previously shown for the $(Cs[5^2D]Xe)^*$ state, is displayed in Figs. 26 and 27. Once again, varying the Xenon pressure affects the amplitude and shape of the emission profile in a greater way than does varying the Cesium density.

C. Discussion of $(Cs[7^2S]Xe)^*$ Data

Due to its large molecular well depth and long radiative lifetime, the $[Cs(7^2S)Xe]^* \rightarrow$ ground excimer band is attractive as a prospective candidate for dissociation lasing. In the discussion to follow, parameters that are essential to determining the feasibility of lasing in CsXe are evaluated. Given the experimental data and conclusions presented above, the collisional and radiative rates that are critical in de-populating the $Cs^*(7^2S)$ and $(Cs[7^2S]Xe)^*$ states have been estimated and are shown in Fig. 28. The processes considered are: 1) three-body $(CsXe)^*$ excimer formation[11,27] $[Cs^*(7^2S) + Xe \xrightarrow{k_f} (Cs[7^2S]Xe)^* + Xe]$; 2) atomic transitions to low lying P states; 3) collisionally - induced atomic fluorescence and 4) excimer spontaneous radiation to the molecular ground state. The three-body excimer formation rate shown is that determined for

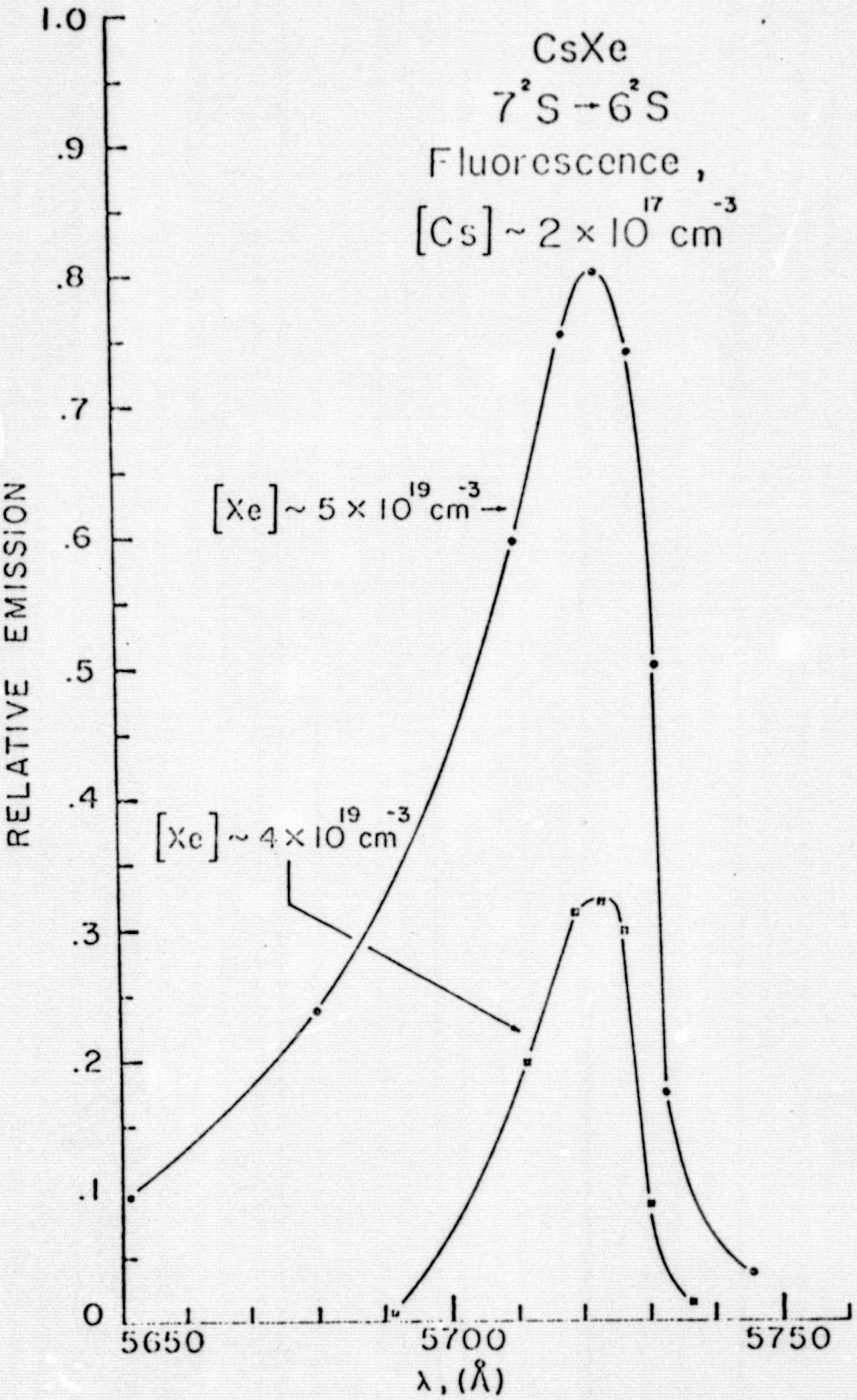

Fig. 26. Xenon pressure dependence of $(Cs[7^2S]Xe)^*$ excimer fluorescence for $[Cs] \sim 2 \cdot 10^{17}\ cm^{-3}$.

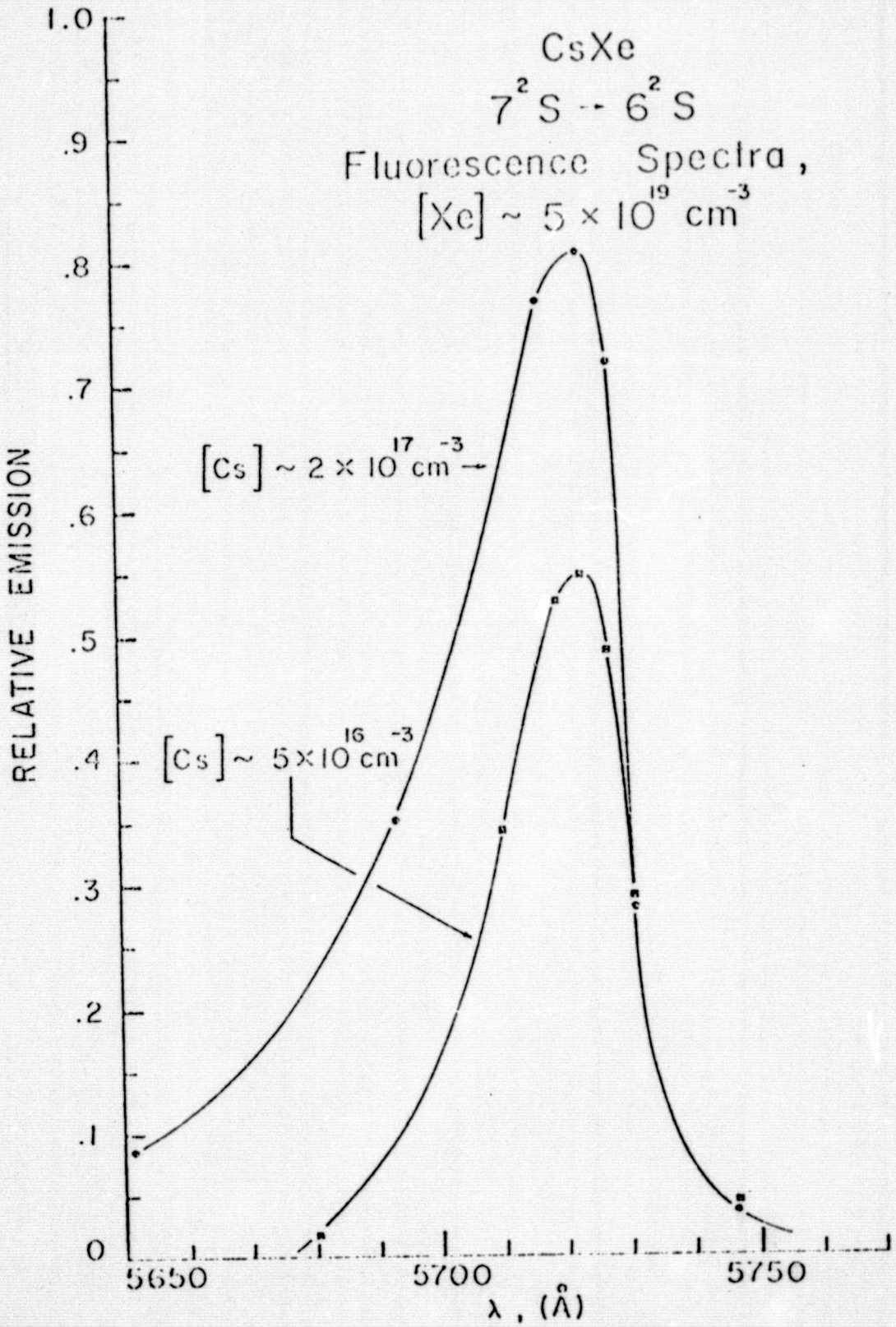

Fig. 27. Cesium density dependence of $(Cs[7^2S]Xe)^*$ fluorescence for $[Xe] \sim 5 \cdot 10^{19}\ cm^{-3}$.

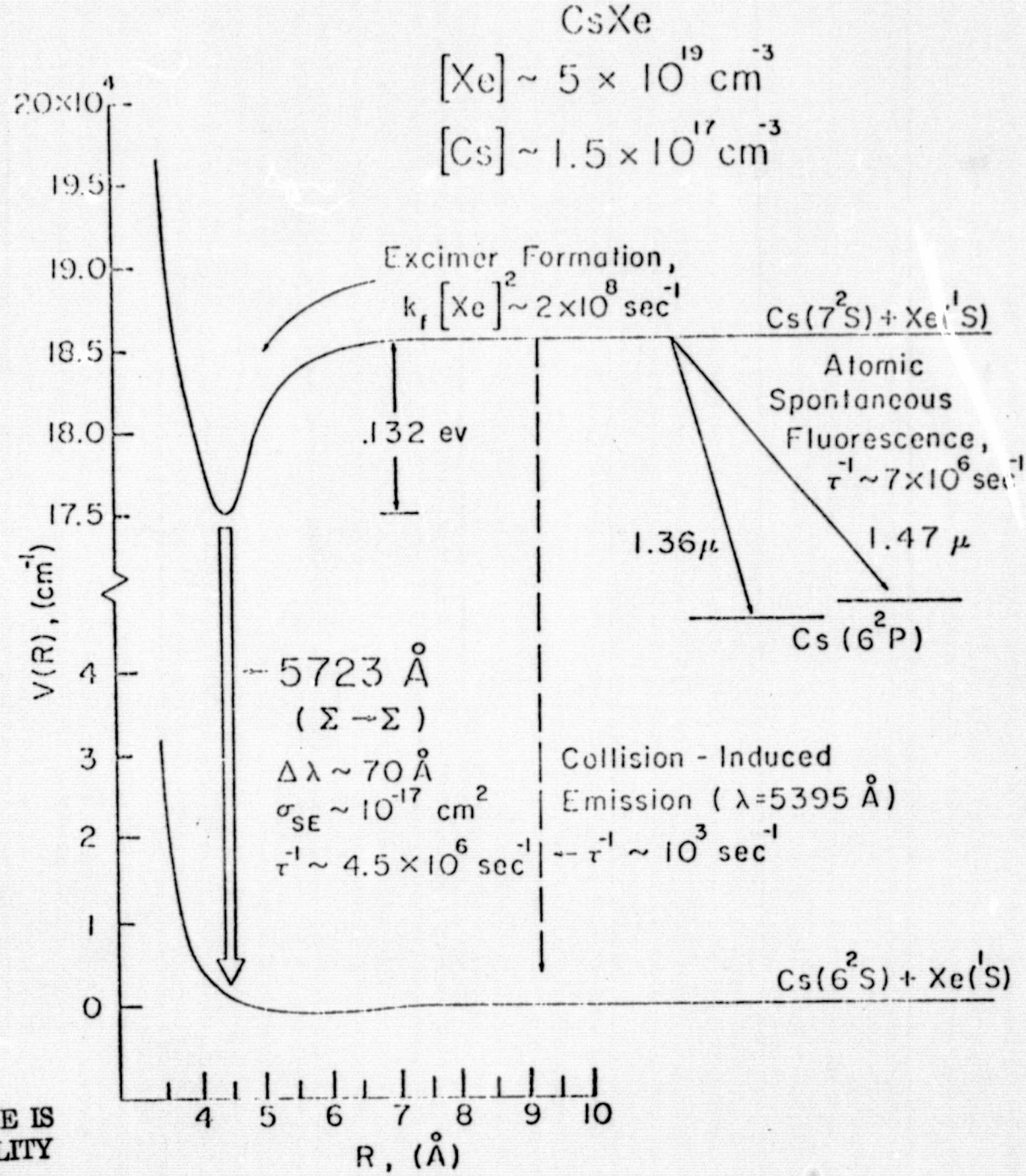

Fig. 28. Energy level diagram of the $Cs^*(7^2S)$ - $(Cs[7^2S]Xe)^*$ atomic-molecular system showing collisional processes important to destroying the $Cs^*(7^2S)$ species. ($[Cs] \sim 1.5 \cdot 10^{17}$ cm^{-3}; $[Xe] \sim 5 \cdot 10^{19}$ cm^{-3}).

RbXe by Carrington and Gallagher to be $k_f = 8.2 \cdot 10^{-32}$ cm^6 - sec^{-1}. From earlier investigations[28] and our studies of this process in NaAr (see Appendix), it has been shown that three-body molecular formation rates vary only slightly among the heavier molecules, such as Xe_2 and RbXe; therefore, our choice of the RbXe value does not significantly affect the validity of our conclusions. So, using Carrington and Gallagher's rate, the three body formation frequency is found to be $\sim 2 \cdot 10^8$ sec^{-1} for [Xe] $\sim 5 \cdot 10^{19}$ cm^{-3} ($\sim$ 2 atm. at room temperature).

Secondly, although radiative transitions are normally not allowed between the $Cs^*(7^2S)$ state and ground, the level is not metastable since it is optically connected to the $Cs^*(6^2P)$ levels through the 1.47 and 1.36μ lines. To estimate the radiative lifetimes for these atomic transitions, note that the spontaneous radiation probability for any allowed optical transition is given by:[29]

$$A_{nm} = \frac{64\,\pi^4\,\nu_{nm}^3}{3h} \left| \langle n \mid \mu \mid m \rangle \right|^2 \qquad (14)$$

where ν_{nm} is the frequency of the transition and $\langle n|\mu|m\rangle$ is the quantum mechanical matrix element discussed earlier. Therefore, assuming the matrix element to be roughly constant for S $\rightarrow$ P lines,

then

$$A_{nm} \sim \lambda_{nm}^{-3} . \tag{15}$$

We may now apply this wavelength dependence to the known transition probability of the $Cs(8^2S_{\frac{1}{2}} \rightarrow 6^2P_{\frac{1}{2}})$ 7609 Å line which is given by Corliss and Bozman[30] as $2.2 \cdot 10^7$ sec^{-1}. Hence:

$$A_{1.36\mu} \simeq 2.2 \times 10^7 \left[\frac{.761}{1.36}\right]^3 \sim 4 \times 10^6 \ sec^{-1}.$$

Similarly, (16)

$$A_{1.47\mu} \simeq 2.2 \times 10^7 \left[\frac{.761}{1.47}\right]^3 \sim 3 \times 10^6 \ sec^{-1}.$$

Therefore, $A_{TOTAL} \sim 7 \cdot 10^6$ sec^{-1} as shown on Fig. 28.

To evaluate the collision-induced atomic fluorescence lifetime at high Xenon densities, the absorption equation in conjunction with the $Cs(6^2S \rightarrow 7^2S)$ experimental absorption data shown earlier yields $\tau_{5395} \sim 1$ msec (at $[Cs] \sim 1.5 \cdot 10^{17}$ cm^{-3}, $[Xe] \sim 5 \cdot 10^{19}$ cm^{-3}), which clearly is negligible with respect to the other destruction rates of interest. (Here, the atomic and molecular spectra FWHM were determined from Fig. 23 to be ~ 60 Å). Similarly, $\tau_{(CsXe)^* 7^2S}$ was found to be ~ 2 μsec.

Finally, Fig. 28 also displays the estimated stimulated emission cross-section for the bound-free $(Cs[7^2S]Xe)^* \rightarrow$ ground excimer transition. From Eq. (4):

$$\alpha(\lambda) = \frac{\lambda^2}{8\pi} \frac{g_U}{g_L} A N_L g(\lambda) \qquad (4)$$

$$= \sigma_{SE} N_L .$$

Then,

$$\sigma_{SE} = \frac{\alpha(\lambda)}{N_L} \qquad (17)$$

where N_L = ground state CsXe density at R_o and $V_U(R_o) - V_L(R_o) = \frac{hc}{\lambda}$. At this point, it might be added that the calculation of the stimulated emission coefficient strongly depends on the shape of the CsXe potential energy level curves. Although the repulsive ground state diagram has been measured accurately by crossed-beam[31] and fluorescence[11] experiments, only theoretical predictions are available for the bound excited molecular states. The upper state shown in Fig. 28 is a modification of the theoretical curve computed by Pascale and Vandeplanque. For reasons stated earlier, we: 1) deepened the potential well to $\sim 1062\ cm^{-1}$ (they predicted a well depth of

$\sim 400\ cm^{-1}$) and 2) shifted the potential minimum from 4.2 to 4.5 Å, where the ground state is only slightly repulsive (see page 21; this modification is necessary to comply with the experimental results of Fig. 25). Using this value of R_{min} and setting $\Delta R = 0.5$ Å, Eq. (7) can be solved to determine the molecular ground state density to be $[CsXe] \sim 10^{15}\ cm^{-3}$. Therefore, $\sigma_{SE} \sim 10^{-17}\ cm^2$, which is of the same order of magnitude as cross-sections evaluated for other promising lasers.[10] It is expected that the ground state density found above is a lower limit and so the actual value of σ_{SE} is possibly smaller than the value given.

Incidentally, it is interesting to note that the 5723 Å excimer continuum results from $\Sigma \rightarrow \Sigma$ transitions of the excited molecule. To our knowledge, all of the dissociation lasers observed to date, including Xe_2^{32}, Xe O[20,21] and Xe F[9], have lased solely on $\Sigma \rightarrow \Sigma$ transitions. This is perhaps significant since, as mentioned earlier, previous investigators have concentrated on utilizing the low lying P states to form the alkali-rare gas excimer state ($\Rightarrow \Pi \rightarrow \Sigma$ transitions).

Given the $(Cs[7^2S]Xe)^*$ excimer absorption linewidth and radiative lifetime presented above, one can readily determine the population inversion necessary to obtain lasing from this molecule. The gain equation may be expressed as:

$$\gamma = \left(N_U - N_L \frac{g_U}{g_L}\right) \frac{\lambda^2}{8\pi} \frac{1}{\tau_{spon}} g(\nu) \quad , \qquad (18)$$

where

$N_{U,L}$ are the molecular excited and ground state population densities, respectively,

$g_{U,L}$ are the molecular excited and ground state degeneracies, respectively,

and

$g(\nu)$ is the absorption lineshape.

Again, approximating the lineshape as the inverse of its linewidth, Eq. (18) may be rewritten as:

$$N_U - N_L = \gamma \frac{8\pi}{\lambda_o^2} \tau_{spon} \Delta\nu \qquad (19)$$

where

$\frac{g_U}{g_L} = 1$,

$\Delta\nu = 6.41 \cdot 10^{12}$ sec^{-1} ($\rightarrow$ 60 Å),

$\lambda_o = 5.723 \cdot 10^{-5}$ cm,

and

$\tau_{spon} \sim 2.2 \cdot 10^{-6}$ sec.

Thus, the 5723 Å excimer transition will have a gain of 1%/m for a population inversion of 10^{13} cm^{-3}. To estimate the excited atomic and molecular densities necessary to produce this inversion, the $(Cs[7^2S]Xe)^*$ molecular-atomic system may be modeled as shown in Fig. 29. Here, the $(Cs[7^2S]Xe)^*$ molecular well is represented by a

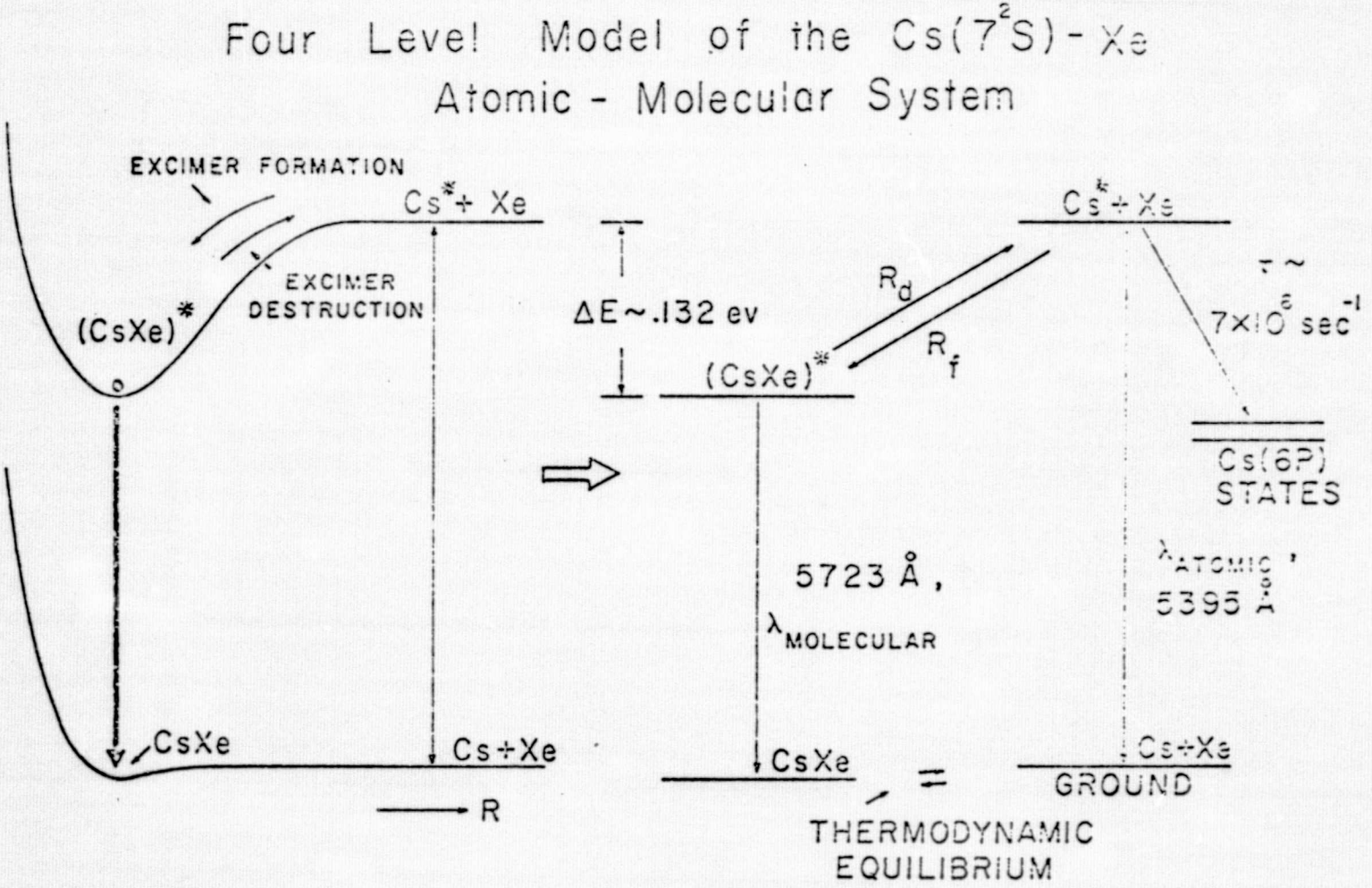

Fig. 29. Four level model of the Cs-Xe system considered.

single level, separated from the $Cs^*(7^2S)$ state by $\Delta E \simeq .132$ eV. Note that the excited atomic-molecular states are coupled by excimer destruction and formation collisions. In the analysis to follow, these rates are assumed to follow from thermodynamic equilibrium considerations. This is surely true as one approaches threshold. Utilizing this simple model, the algebraic equations describing the interrelation of the various particle densities may be expressed as follows. Given the ground state densities [Cs] and [Xe], then from Eq. (7), the CsXe ground state molecular population at a specified interatomic radius R_o and radial interval ΔR is given by:

$$[CsXe] \simeq 4\pi R_o^2 [Cs][Xe] \Delta R \exp\left\{-\frac{\Delta E}{kT}\right\} \quad (7)$$

where $\Delta E \equiv \left|V_L(R_o) - V_L(\infty)\right| \lesssim \frac{kT}{4}$

and T = gas temperature.

Substituting $R_o = 4.5$ Å, $\Delta R = 0.5$ Å (the values chosen earlier to calculate σ) and kT (600° K) $\simeq .05$ eV into Eq. (7), the result is:

$$[CsXe] = 1.27 \times 10^{-22} [Cs][Xe] \ , \ cm^{-3}. \quad (20)$$

Secondly, the molecular excited and ground state densities are related through Eq. (19):

$$[CsXe]^* - [CsXe] \simeq 10^{13} \ cm^{-3} . \quad (21)$$

This relation yelds the threshold inversion necessary to obtain lasing. The differential equation describing the time rate of change of the excimer population, $[CsXe]^*$, is given by:

$$\frac{d[CsXe]^*}{dt} = - R_d [CsXe]^* + R_f [Cs]^* - \tau_{mol}^{-1} [CsXe]^* \qquad (22)$$

where R_d and R_f are expressed in sec^{-1} and stimulated emission losses are assumed to be negligible. The steady-state solution of Eq. (22) is:

$$[CsXe]^* = \frac{R_f}{R_d} [Cs]^* \qquad (23)$$

where $\tau^{-1}_{MOLECULE} \sim 4.5 \cdot 10^6$ $sec^{-1} \ll R_d$, as will be shown later. Since R_d is extremely difficult to isolate experimentally, chemical kinetics may be employed to estimate the ratio $\frac{[CsXe]^*}{[Cs]^*}$.

The steady-state chemical reaction:

$$(CsXe)^* + Xe \underset{R_f}{\overset{R_d}{\rightleftharpoons}} (Cs)^* + Xe + Xe \qquad (24)$$

is characterized by the equilibrium constant K(T), (T = gas temperature), that is defined by:

$$K(T) = \frac{[CsXe]^*}{[Cs]^* [Xe]} \quad . \tag{25}$$

From statistical mechanics, Eq. (25) may be written as:

$$\frac{[CsXe]^*}{[Cs]^* [Xe]} = Q_t \, Q_r \, Q_v \, Q_e \tag{26}$$

where Q_t, Q_r, Q_v and Q_e are the translational, rotational, vibrational and electronic partition functions for the diatomic $[CsXe]^*$ molecule. It can be shown[33] that

$$Q_t = \left[\frac{h^2}{2 \pi k T} \left(\frac{m_{CsXe}}{m_{Cs} \; m_{Xe}} \right) \right]^{\frac{3}{2}}$$

where m is the mass of the specified particle

and $$Q_e = \exp \left\{ D / kT \right\} ,$$

D = molecular dissociation energy = 1062 cm^{-1} for the $(Cs[7^2S]Xe)^*$ state.

Also, Q_r and Q_v may be approximated as:[29]

$$Q_r \simeq \frac{kT}{B}$$

where B = rotational constant = $\frac{h^2}{8 \Pi^2 I}$,

I = moment of inertia,

and $$Q_v = \frac{\exp(-\theta/2T)}{1 - \exp(-\theta/T)}$$

where $\theta = \frac{h\omega}{2 \pi k}$,

$\omega = (\kappa/\mu)^{1/2}$ (κ is the molecular force constant and μ is the reduced mass of the molecule).

As a result, Eq. (26) may be re-expressed as:

$$\frac{[CsXe]^*}{[Cs]^* [Xe]} \simeq \left[\frac{h^2}{2\pi kT} \left(\frac{m_{CsXe}}{m_{Cs} m_{Xe}} \right) \right]^{\frac{3}{2}} e^{\frac{D}{kT}} \frac{kT}{B} \frac{\exp\left\{-\frac{\theta}{2T}\right\}}{1 - \exp\left\{-\frac{\theta}{T}\right\}} \cdot \quad (27)$$

From the periodic chart,

$$m_{Cs} \simeq m_{Xe} = 2.2 \cdot 10^{-22} \frac{\text{grams}}{\text{atom}}$$

and setting

$$r_{CsXe} \simeq r_{Cs} + r_{Xe} \simeq 10 \text{ Å},$$

then I may be shown to be $1.1 \cdot 10^{-36}$ gm - cm^2.

Thus, the rotational constant $B \simeq 5 \cdot 10^{-26}$ joules.

Given a gas temperature of 600° K,

$$Q_r = 1.66 \cdot 10^5.$$

Also, since

$$D = 1062 \text{ cm}^{-1} = .132 \text{ eV},$$

then

$$Q_e = e^{D/kT} = 12.74.$$

If $m_{CsXe} = m_{Cs} + m_{Xe}$,

then $Q_t = 6.65 \cdot 10^{-28}$ cm^3.

To find Q_v, it is necessary to determine $\hbar\omega$, where $\omega \sim \mu^{-1/2}$, μ = reduced mass of the molecule. Yardley[33] gives $\hbar\omega = 100$ cm^{-1} for the $(NaXe)^*$ molecule.

Therefore, $\frac{\hbar\omega_{CsXe}}{\hbar\omega_{NaXe}} \sim \left(\frac{\mu_{NaXe}}{\mu_{CsXe}}\right)^{1/2} = \left(\frac{3.25 \cdot 10^{-23}}{2.2 \cdot 10^{-22}}\right)^{1/2} = .384.$

Hence, $\hbar\omega_{CsXe} = 38.4$ cm^{-1} $\Rightarrow \theta = 57.5\ ^{\circ}K$.

As a result,

$$Q_v = 10.4$$

and so

$$Q_{TOTAL} = Q_t\, Q_v\, Q_r\, Q_e = 1.46 \cdot 10^{-20} \text{ cm}^3.$$

Substituting this result into Eq. (26), we have:

$$\frac{[CsXe]^*}{[Cs]^*\,[Xe]} = 1.46 \times 10^{-20} \text{ cm}^3. \qquad (28)$$

At first glance, Eq. (28) is surprising since for [Xe] $\cdot$ $6.85 \cdot 10^{19}$ cm^{-3}, the excited atomic population exceeds that of the excimer. However, it must be remembered that the translational "density of states" for the excited Cesium state is huge. Thus, high Xenon densities are required for the chemical reaction (Eq. (24)) to favor

formation of the $(CsXe)^*$ excimer. One flaw of the method presented above to determine $\frac{[CsXe]^*}{[Cs]^*\,[Xe]}$ is that Eq. (27) tends to overestimate Q_r and Q_v for shallow molecular wells (D ~ a few kT). The uncertainty introduced by this problem is, however, expected to be small.

Finally, the total number of Cesium atoms in this system must be conserved.

Hence:

$$[Cs] + [CsXe] + [CsXe]^* + [Cs]^* = [Cs]_{TOTAL} \qquad (29)$$

where $[Cs]_{TOTAL}$ is the Cesium density corresponding to the gas temperature, T.

Equations (20), (21), (28) and (29) may be solved simultaneously for the densities [Cs], [CsXe], $[CsXe]^*$ and $[Cs]^*$:

$$[Cs] = \frac{[Cs]_{TOTAL} - 10^{13}\left\{1 + \frac{6.85\times10^{19}}{[Xe]}\right\}}{1 + 1.27\times10^{-22}[Xe]\left\{2 + \frac{6.85\times10^{19}}{[Xe]}\right\}} \qquad (30)$$

$$[CsXe] \simeq 1.27\times10^{-22}[Cs][Xe] \quad , cm^{-3} \qquad (31)$$

$$[CsXe]^{*} = [CsXe] + 10^{13}\ cm^{-3} \tag{32}$$

and

$$[Cs]^{*} = \frac{6.85 \times 10^{19}}{[Xe]} \left\{ 1.27 \times 10^{-22}\ cm^{3} [Cs][Xe] + 10^{13}\ cm^{-3} \right\} . \tag{33}$$

If $[Cs]_{TOTAL} \simeq 1.5 \cdot 10^{17}\ cm^{-3}$ and $[Xe] = 5 \cdot 10^{19} cm^{-3}$ are substituted into Eqs. (30) - (33), the results are

$$[Cs] \simeq 1.47 \cdot 10^{17}\ cm^{-3},$$

$$[CsXe] \simeq 9.3 \cdot 10^{14}\ cm^{-3},$$

$$[CsXe]^{*} \simeq 9.43 \cdot 10^{14}\ cm^{-3}$$

and $$[Cs]^{*} \simeq 1.29 \cdot 10^{15} cm^{-3}.$$

One collisional process that has not been incorporated into the atomic-molecular model is $[Cs]^{*} - [Cs]^{*}$ collisional ionization. Although the cross-section for this process is presumably large[34] ($> 10^{-15}\ cm^{2}$), the low $[Cs]^{*}$ density calculated causes this loss mechanism to be small compared to the atomic radiative decay processes. Finally, it is significant that the ground atomic state density must be depleted by $\sim 2\%$ to obtain the required $[Cs]^{*}$ population.

To determine the feasibility of obtaining stimulated emission from the $(Cs[7^2S]Xe)^*$ excimer, it is desirable to calculate the critical fluorescence power. This is the power that must be delivered to the gaseous medium for the $(Cs[7^2S]Xe)^* \rightarrow$ ground molecular transition band to be optically transparent (i.e., absorption = gain $\equiv$ 0). To calculate this power from the excited atomic and molecular densities, we have:

$$P_c = h\nu_a A_a [Cs]^* + h\nu_m A_m [CsXe]^* \quad (34)$$

where $\nu_{a,m}$ are the center frequencies of the atomic and molecular fluorescence, respectively, and $A_{a,m}$ are the spontaneous radiative rates for the atomic and molecular transitions.

Setting: $h\nu_a = 2.3$ eV (5395 Å),

$h\nu_m = 2.17$ eV (5723 Å),

$A_a \simeq 7 \cdot 10^6$ sec^{-1},

$A_m = 4.5 \cdot 10^5$ sec^{-1},

$[Cs]^* = 1.29 \cdot 10^{15}$ cm^{-3}

and

$[CsXe]^* = 9.43 \cdot 10^{14}$ cm^{-3}, then the critical fluorescence power becomes $P_c = 3.46$ kw/cm^3, for $[Cs]_{TOTAL} = 1.5 \cdot 10^{17}$ cm^{-3} and $[Xe] = 5 \cdot 10^{19}$ cm^{-3}. The critical fluorescence power may also be defined as the power input necessary to attain lasing threshold. However, once stimulated emission is initiated, thermodynamic

equilibrium between the $[CsXe]^*$ and $[Cs]^*$ populations is destroyed and so any additional power delivered to the $[Cs]^* - [CsXe]^*$ system will be converted to stimulated emission energy. It is also important to note that the value of P_c computed above depends on the excimer potential energy curves, which have not been verified experimentally.

The dependence of the critical fluorescence power density on Xenon pressure for a fixed Cesium density is displayed in Fig. 30. A distinct minimum of the required input energy occurs at $[Xe] \sim 3 \cdot 10^{19}$ cm^{-3}. This minima is to be expected due to the following competing effects: 1) P_c rises at low pressures since, in this regime, the equilibrium condition (Eq. 28) favors the formation of the $(Cs)^*$ excited atom (rather than the excimer), and 2) again climbs steeply at increasing [Xe] since [CsXe] and hence, $[CsXe]^*$ (implies larger threshold power), varies directly with the Xenon density.

Thus, for the $(Cs[7^2S]Xe)^* \rightarrow (Cs[6^2S]Xe)$ excimer continuum, laser gain is expected for small inversion densities. In addition, this excimer state is characterized by: 1) a high stimulated emission cross-section, $\sigma \sim 10^{17}$ cm^2/excited molecule; 2) a relatively long radiative lifetime (2 μsec) as compared to the alkali-rare gas Π states and 3) excimer $\rightarrow$ ground $\Sigma \rightarrow \Sigma$ transitions that are common to the dissociation lasers found to date. Finally, the power input/cm^3 to reach laser threshold is well within the grasp of present experimental techniques. These characteristics qualify

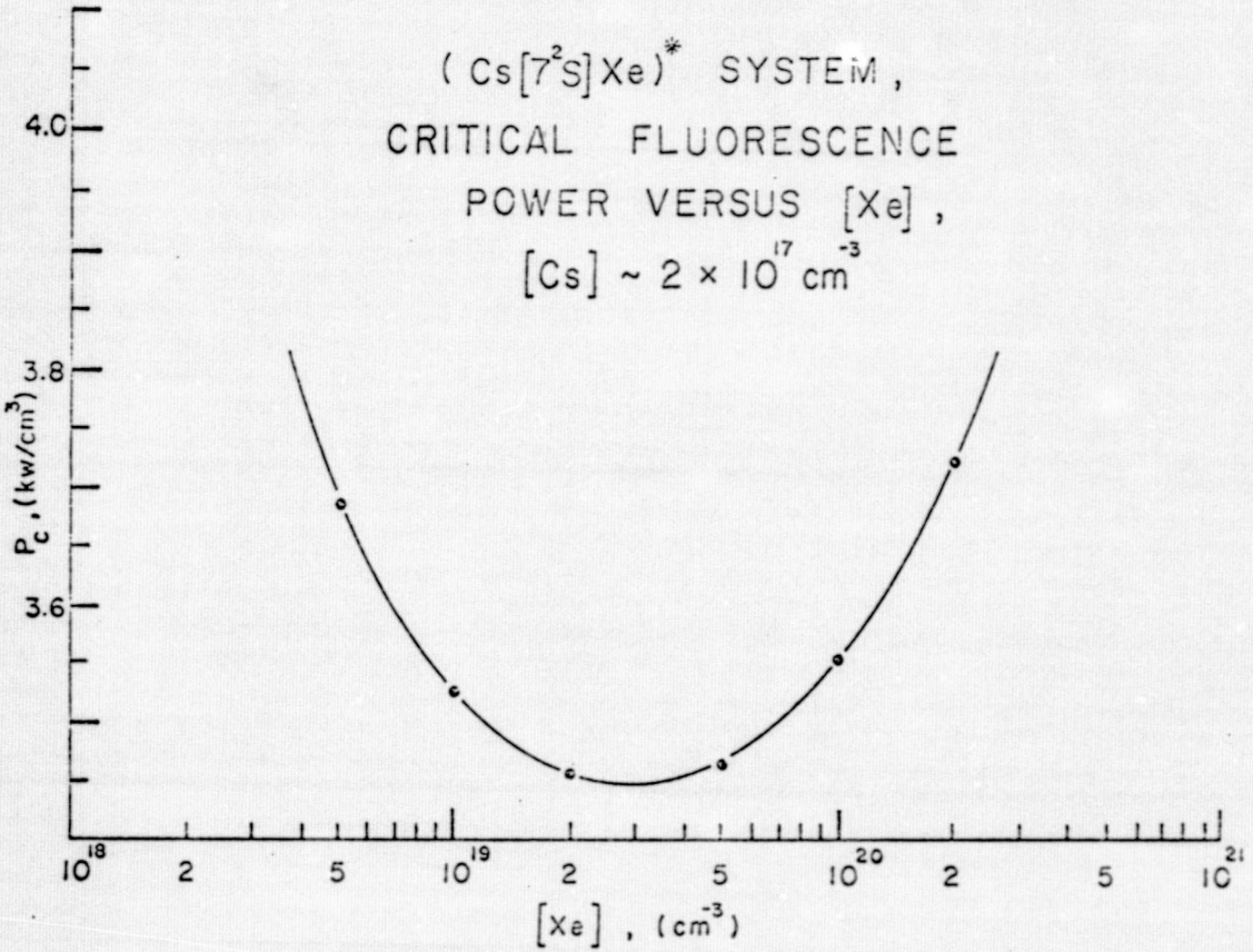

Fig. 30. Variation of the Critical Fluorescence Power as a function of the Xenon perturber density.

the Cs^* (7^2S) - Xe(^1S) atomic-molecular system as one of the most attractive potential dissociation laser molecules under investigation at present.

IV. CONCLUSIONS AND SUGGESTIONS FOR FURTHER WORK

By measuring the absorption and emission continua of various states in the Cesium-Xenon molecule, the collisional rates critical in populating the alkali-rare gas excimer levels have been estimated. In contrast to previous investigations of this molecule, Cs-atomic states that are weakly optically connected to ground have been studied and have been shown to form excimer levels that are attractive as potential dissociation lasers. Due to the long spontaneous radiative lifetimes of these Cesium atomic states, the excimer formation rate, $k_f[Xe]^2$, dominates excited atomic radiative losses for Xenon gas densities in excess of $\sim 10^{19}$ cm^{-3}.

In particular, the $(Cs[7^2S]Xe)^*$ excited molecule appears promising as a source of high energy laser radiation due to its large dissociation energy, stimulated emission cross-section, and small population inversion densities.

Significant gaps in our knowledge of the physical properties of these molecules remain, however. Further investigation into the potential energy profiles, dissociation energies and collisional deactivation rates of the alkali-rare gas excimers is necessary. For example, by optically pumping the 4418 Å $Cs(6^2S_{1/2} - 6^2D_{5/2})$ transition using the He-Cd 4416 Å laser line in the presence of Xenon, monitoring the resulting fluorescence would provide a direct means of measuring the well depth of the $(Cs[6^2D]Xe)^*$ molecular states.

Also, as more information concerning the structure of these excimers becomes available, detailed modeling of potential laser systems, such as the one discussed here, would be desirable.

In order to produce lasing in these systems, flashlamp pumping ought to be pursued. Careful gain measurements of the gaseous medium conducted for various lamp currents, Cesium and Xenon densities would provide valuable insight into the feasibility of obtaining stimulated emission from the $(Cs[7^2S]Xe)^*$ excimer.

Finally, although not mentioned earlier, while measuring the absorption spectra of the CsXe molecule, the absorption of Cs_2 molecules was simultaneously monitored. It was surprising to discover that the Cs_2 C band (6200-6400 Å) absorption profile changed drastically with increasing Xenon pressure as shown in Fig. 31. Clearly, dominant absorption at large Xenon densities is centered around ~ 6380 Å as opposed to 6300 Å for lower perturber pressures.[13] Studies of the collisional mechanisms responsible for this phenomenon would be valuable.

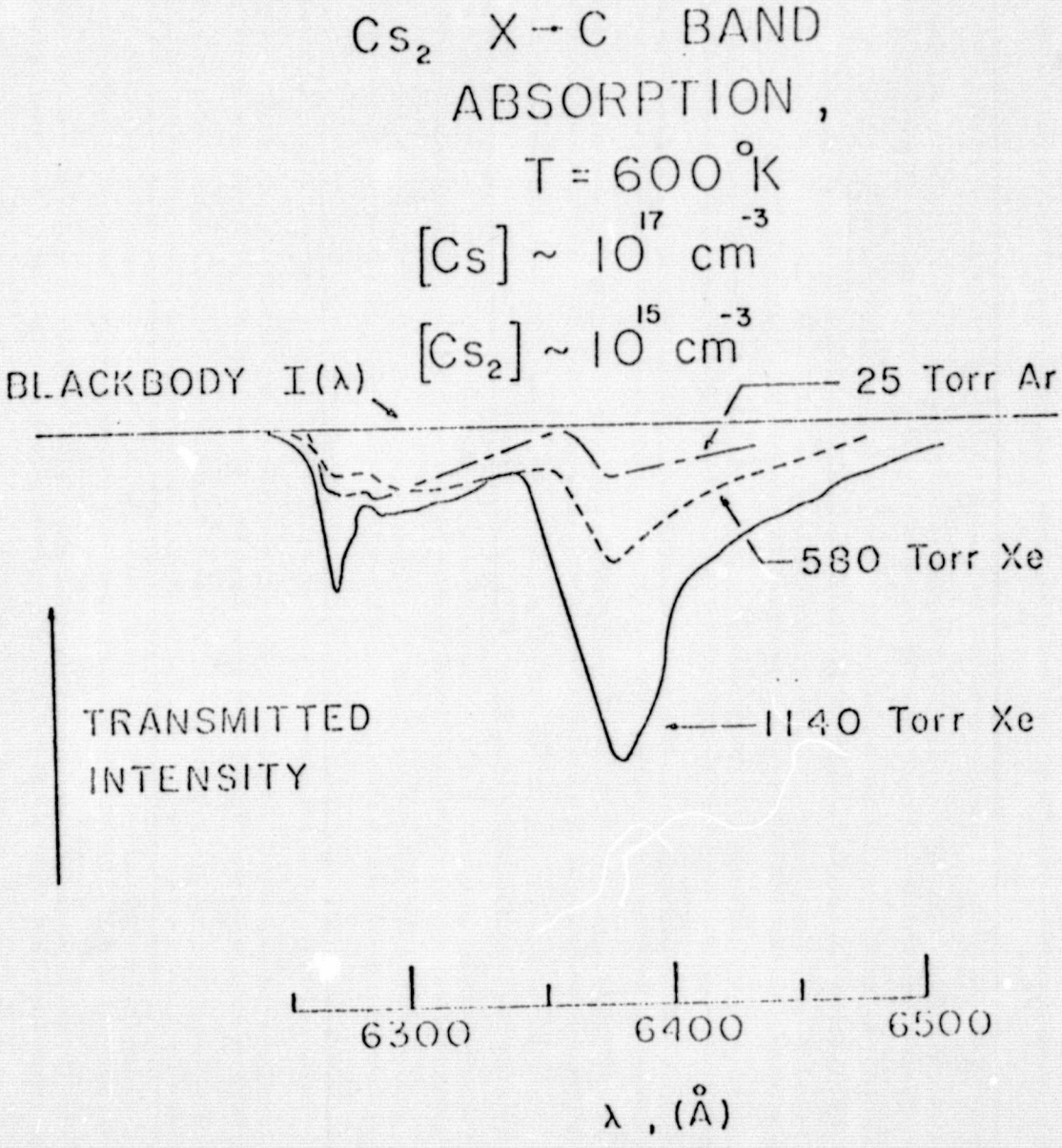

Fig. 31. Absorption spectra of the Cs_2 X → C band for various rare-gas pressures showing peak absorption at ~ 6380 Å for high Xenon pressures.

REFERENCES

[1] F.G. Houtermans, Helv. Phys. Acta. 33, 933 (1960).

[2] N.G. Basov, V.A. Danilychev and Yu.M. Popov, Sov. J.Q.E. 1, 18 (1971).

[3] J.B. Gerardo and A. Wayne Johnson, IEEE J.Q.E. QE-9, 748 (1973).

[4] H.A. Koehler, L.J. Ferderber, D.L. Redhead and P.J. Ebert, Appl. Phys. Lett. 21, 1968 (1972).

[5] P.W. Hoff and C.K. Phodes, paper C-2, 26th Gaseous Electronics Conference, Madison, Wisconsin (1973).

[6] H.T. Powell, J.R. Murray and C.K. Rhodes, Appl. Phys. Lett. 25, 730 (1974).

[7] S.K. Searles and G.A. Hart, Appl. Phys. Lett. 27, 243 (1975).

[8] J.J. Ewing and C.A. Brau, Appl. Phys. Lett. 27, 350 (1975).

[9] C.A. Brau and J.J. Ewing, Appl. Phys. Lett. 27, 435 (1975).

[10] A.V. Phelps, JILA Report #110, September, 1972.

[11] R.E.M. Hedges, D.L. Drummond and A. Gallagher, Phys. Rev. A 6, 1519(1972); D.L. Drummond and A. Gallagher, J. Chem. Phys.60, 3426 (1974).

[12] M. Lapp, Phys. Lett. 23, 553 (1966).

[13] M. Lapp and L.P. Harris, J. Appl. Phys. 34, 3622 (1963); ibid, J. Quant. Spectrosc. Radiat. Transfer 6, 169 (1966). Weak absorption was observed here for the Cs(5^2D) states, but was not attributed to collision induced absorption. In fact that phenomenon was not mentioned.

[14] F. Besombes, J. Granier and R. Granier, Opt. Comm. 1, 161 (1969).

[15] J.A. Gwinn, P.M. Thomas and J.F. Kielkopf, J. Chem Phys. 48, 568 (1968).

[16] A. Tam, G. Moe, W. Park and W. Happer, Phys. Rev. Lett. 35, 85 (1975).

[17] L. Noble, C. Kretschmer, R. Maynard, H. Flentz and L. Reed, Research and Development Report, U. S. Army Electronics Command (Ft. Monmouth, N.J. 07703), ECOM-0239-F (1973), pp. 36, 62.

[18] D. E. Freeman, K. Yoshino and Y. Tanaka, Paper OA-8, 28th Gaseous Electronics Conference, Rolla, Missouri, October, 1975.

[19] D.E. Gilbert and S.Y. Ch'en, Phys. Rev. 188, 40 (1969) and references quoted therein.

[20] D.L. Cunningham and K.C. Clark, J. Chem. Phys. 61, 1118 (1974).

[21] H.T. Powell, J.R. Murray and C.K. Rhodes, Paper 7.8, 1975 CLEA Conference, Washington, D.C.

[22] C. Tai, W. Happer and R. Gupta, Phys. Rev. A 12, 736 (1975).

[23] C.L. Chen and A.V. Phelps, Phys. Rev. A 7, 470 (1973).

[24] J. Pascale and J. Vandeplanque, J. Chem. Phys. 60, 2278 (1974).

[25] C.E. Treanor, J.W. Rich and R.G. Rehm, J. Chem. Phys. 48, 1798 (1968).

[26] W.Q. Jeffers and J.D. Kelley, J. Chem. Phys. 55, 4433 (1971).

[27] C.G. Carrington and A. Gallagher, J. Chem. Phys. 60, 3436 (1974).

[28] R.T. Ku, J.T. Verdeyen, B.E. Cherrington and J.G. Eden, Phys. Rev. A 8, 3123 (1973) and references cited therein.

[29] G. Herzberg, Molecular Spectra and Molecular Structure I. Spectra of Diatomic Molecules, Van Nostrand Reinhold Co., New York (1950).

[30] C.H. Corliss and W.R. Bozman, NBS Monograph 53, 79 (1962).

[31] C.J. Malerich and R.J. Cross, Jr., J. Chem. Phys. 52, 386 (1970).

[32] E.V. George and C.K. Rhodes, Appl. Phys. Lett. 23, 139 (1973).

[33] J.T. Yardley, Statistical Mechanics and Dimer Formation, (unpublished) 1973.

[34] P.A. Miller, J.T. Verdeyen and B.E. Cherrington, Phys. Rev. A 4, 692 (1971).